Università degli Studi di Padova
Facoltà di Ingegneria

Corso di Laurea Magistrale in Ingegneria delle Telecomunicazioni

Tesi di Laurea Magistrale

The Heartbeat Evoked Field evaluation & analysis

Candidato:
Marco Gambarotto
Matricola 1043602

Relatore:
Silvano Pupolin

Correlatore:
David J. Liley

Anno Accademico 2014–2015

To Riccardo, Stefania, Stefano and Ji Won

Contents

Introduction

This thesis is the result of a research project performed during an internship at the Brain and Psychological Sciences Research Center (BPsyC) of the Swinburne University of Technology in Melbourne.
The aim of this work is to evaluate the "pure" Heartbeat Evoked Field (HEF). The HEF is the magnetic field generated by the Heartbeat Evoked Response, basically the cortical feedback to the heartbeat, and recorded through the MEG. The term "pure" refers to the approach of comparing the cortical response to the heartbeat against a null baseline, which is the innovation introduced in this work: in fact in the literature there is a lack of a pure Heartbeat Evoked Response evaluation, since every study evaluates the difference in the HER between different experimental conditions, assuming a priori the existence of such response. However the HER has never been isolated and evaluated, although it is a physiological signal with many interesting medical outcomes.
The study is structured in two main branches: the sensor analysis and the source analysis. The aim of the first is to retrieve temporal and topographical information about the target response through a direct processing of the MEG data (collected at the BPsyC), while the aim of the latter is to obtain an estimation of the neuronal sources significantly activated by the heartbeat stimulus.
This work is organized as following: the first part is focused on providing the physiological background about the HER and the experimental scenario. Then the mathematical model of the sensor analysis signals is described, followed by the detailed processing protocol and the respective results, with a focus on some issues and their fixation. The last chapter is then dedicated to the source analysis.
The software used to obtain the results and to visualize them was MatLab and a MatLab-based toolbox called FieldTrip.

Chapter 1

The Heartbeat Evoked Field

1.1 Definition of HEF

Measures of the brain's electrical activity, generally either on-going activity or evoked potentials, are used to study human perceptual and cognitive processes. Evoked potentials are the small changes in voltage that are time-locked to stimulus or cognitive events, and are thought to represent the processing of the information contained in those stimuli or the cognitive events. In case of MEG recording, such quantity is physically an Evoked Field, but the meaning is the same. That is why, in general, they are called Evoked Responses.
When the stimulus is the heartbeat, such changes, or responses, are called Heartbeat Evoked Response (HER). Thus the HER is essentially the impulse response of the brain to the heartbeat and it is a marker of the cortical representation of cardiac information: at each heartbeat, mechanosensory receptors in the heart and aortic walls transiently discharge at specific phases of the cardiac cycle. This information can be relayed up to the neocortex, with ascending anatomical pathways targeting numerous cortical structures, including the posterior insula, ventral anterior cingulate cortex (vaCC), amygdala and somatosensory cortex [1].

1.2 The physiological pathways

The brain processes a continuos stream of information about the environment, both the external environment and the internal environment of the body. This info is supplied by the peripheral nervous system, which though anatomically separate from the central nervous system (CNS), is functionally interwined with it. In order to be able to carry out a significant HER evaluation, and then to infere consistent clinical results, it is definitely interesting to depict the communication scenario between the brain and the heart.
A prominent source of cardiac afferent signal arises from low threshold baroceptors and mechanoreceptors of the ventricular myocardium, carotid sinus, and aortic arch. These respond to stretch, compression, and deformation, thereby signalling information about cardiac filling and function. This information is conveyed centrally along vagus nerve and spinal afferents to influence centrally mediated cardio-cardiac reflexes. An important feature of baroceptor-mediated information is that it occurs

in a cyclical fashion in time with the cardiac cycle.
Human and animals studies suggest the cardiac afferent information is relayed hierarchically through the CNS by nucleus of the solitary tract, medulla, parabrachial nucleus, hypothalamus, and thalamus. In particular, the nucleus of the solitary tract distributes visceral sensory information within the brain along three main pathways:

1. Some neurons in the nucleus of the solitary tract directly innervate preganglionic neurons in the medulla and spinal cord, triggering direct autonomic reflexes.

2. Other neurons in the nucleus project to the lateral medullary reticular formation, where they engage populations of premotor neurons that organize more complex, patterned autonomic reflexes. For example, groups of neurons in the rostral ventrolateral medulla control blood pressure by regulating both blood flow to different vascular beds and vagal tone in the heart to modulate heart rate.

3. The third main projection from the nucleus of the solitary tract provides visceral sensory input to a network of cell groups that extend from the pons and mid brain up through the hypothalamus, amygdala, and cerebral cortex.

Indeed the third is the most important for the HER evaluation, especially the pathways concerning the cerebral cortex. Here, the target structures are the somatosensory cortex, the ventral anterior cingulate cortex (vACC), and the insular cortex. In particular, homeostatic afferent information is conveyed by both basal and posterior ventromedial thalamic nuclei to the superior margin of the insula cortex, which supports a cortical representation of visceral state. Mid-and-posterior insula regions appear to map physiological afferent information in an anatomically graded somatopic mapping of the viscera.
In [10] it is thought that the insular cortex is a most probable source of brain activity being triggered by cardio-afferent signals: it is a well established finding that this region plays an important role for the regulation of cardiovascular activity. Using functional imaging, it can be demonstrated that increased neuronal activity in the insular cortex is associated with cardiovascular arousal.

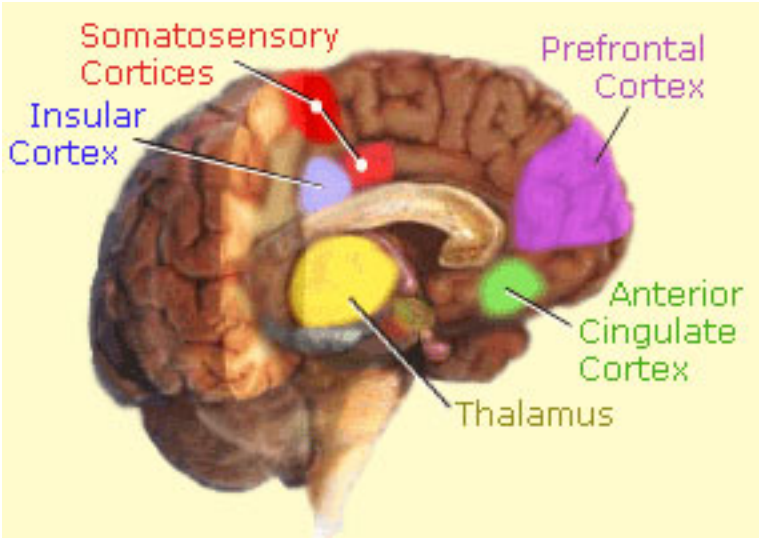

Figure 1.1: Brain section.

1.3 The importance of the HEF

The investigation about the evoked responses is justified by several reasons, which are divided in two main set: the cogntive processes survey and the clinical purpose.
Example of works belonging to the first set can be found in [3], where it is stated that HEP measures seem to have a great deal of face validity as a measure of mental workload, so cognitive overload should directly affect brain functions and the related electrical activity; or in [6], where it is stated that the registration of cardiac-related brain activity is a useful tool in investigating psychophysiological and neuroanatomical questions of visceroceptive information processing.
On the other side, the physiological pathways generating the evoked responses offer new ways in the diagnostic procedures: in fact, evaluating the HER trend may be helpful to identify a particular pathology, or at least it might offer an objective measure of subjective symptom.
For example, the HEP can help in accurate pain assessment since some recent studies have shown that pain-related evoked potential and pain rating can be modulated across the cardiac cycle, probably due to a close integration of the pain system and the neural network involved in cardiovascular regulation. There is also emerging evidence that afferent signals from the heart can modulate pain perception through the neural pathways including the periaqueductal grey matter (PAG), the thalamus, the hypothalamus, the amygdala and the prefrontal cortex. There are therefore close neuronal links between pain perception and central processing of cardiovascular activity. Hence it is reasonable to hypothesize that the brain electrical activity associated with the processing of cardio-afferent input, i.e. the HEP, may refelect pain processing in the brain and offer potential use for pain assessment [5].
Furthermore, HEP can be useful in diagnosis of myocardial functions and dysfunctions during induced stress. In particular, stress challenge would evoke changes in cardiac output, heart wall motion, and electrophysiological homogeneity, in accordance with the nature and extent of cardiac pathology, and that cortical HEPs would: reflect afferent cardiac information, predict functional impairment in these cardiovascular patients, and predict proarrhythmic ECG changes in response to stress [2].

1.4 Localization of the HEF

A key point in the HER evaluation is indeed its topography, that is which brain areas are more proned to have a significant voltage change locked to an internal stimulus. Since the brain is a very complex network, it is trivial that it will not be equally involved in a particular stimulus processing, but just few areas will be relevant for the target analysis. Thus, being an EEG/MEG data recording carried out through a high number of sensors, each corresponding to a particular cortex region, it is essential to identify the active areas in order to evaluate significant time course trend of the evoked response.

In the HER case, there is an apparent lack of topography consistency across studies, since the HER regions reported in the literature are quite different, going from the frontal cortices to the temporal ones. The main causes of such non homogeneity are mainly the time window and the kind of condition considered.
The time plays an important role in the HER evaluation: since the main challenge in such analysis is the superimposition of ECG waveform, generated within the myocardium, across the scalp sensors, it is basic to consider a time range in which the heart artifact is almost negligible. However, the time windows in the literature are very different and this is definitely a reason why the reported topography is so uneven: as a matter of fact, during this study was observed that changing the time window of interest even in a simply rest condition (in particular, the Eyes-Open one), the changes in the topography were astonishing. This is due to the fact that the heartbeat generates an electric voltage conveyed to the cortex through physiological pathways and lasting on average $300ms$ after the R wave. Thus, focusing in a too early time window means evaluating an ECG artifact rather than an actual brain information processing.
Futhermore, the type of experiment must be considered too: even though the heartbeat feedback processing may be expected to be localized in certain areas, it should be also taken account that the brain high complexity can cause a correlation between the processing due to an external stimulus or a task and the cortical processing due to the heartbeat, causing an overall activation of different regions. Finally, it has to be noted that there is not a consistency neither in the type of baseline (rest) condition, since every study used a different one.
By the way here it is report the state of the art in the topography, considering also the time window and the task adopted:

- In [6] the experiment is composed by a task in which the subject has to count his/her own heartbeats and another in which he has to attend to a series of tones; the time window considered is [350 550]ms after the R wave. The topography is evaluated in the time windows of [350 450]ms and [450 550]ms, separately for each condition and showing the average recorded voltage. The results localize the HEP mainly in the frontal and central regions.

- In [5], the subjects have to go through three conditions: the no-task control (in which the subject has simply to relax and stay awake), the no-pain condition (where the subject is required to immerse his/her non-dominant hand in $25°C$ water and in the meanwhile carrying on a backwards counting task) and the cold pain condition (where the subject is asked to immerse his/her non-dominant hand into $10°C$ water). The time window considered is [200 600]ms after the R peak, but showing the topography of the recorded voltage for each condition at every $100ms$. The result is a HEP notable over the frontal and central scalp regions in both control conditions.

- In [2], a mental stress task (serial seven subtraction task) is compared against a baseline condition during which the subjects are simply required to count aloud from 1 to 50 in a regular and relaxed fashion. The computation time slot is [455 595]ms after the R wave and two main kinds of topography are evaluated: the average difference of HEP voltage difference between stress and

baseline condition, and the association (given by the $t - statistic$) between HEP and cardiac output/cardiac repolarization homogeneity. In the first case, no significant difference is observed, while in the latter it can be seen that the HEPs at left temporal and lateral prefrontal surface electrodes are the most correlated with the cardiac output.

- In [1] the experiment consists in the detection of a visual stimulus after a warning one, so the two conditions considered are the hit or the miss of the visual stimulus by the subject, evaluating the HEF (since the MEG is used) corresponding to the heartbeat during the warning interval right before the target visual stimulus. The time window chosen is [350 700]ms after the R wave, then refined to [435 471]ms and the topography considered is the difference between the HEF amplitude of hits and misses cases. The result shows such difference greater in the frontal and parietal regions of the right hemispheres. Finally, reconstructing the neural sources of MEG activity separately in hits and misses, two regions result consistently differentially activated: one extending across the vACC and ventromedial prefrontal cortex bilaterally, and another in the posterior part of right inferior parietal lobule in the angular gyrus.

- In [7] the subjects are simply required to watch a silent movie, sitting in a comfortable position, during the entire recording time. The time window selected for the HEP evaluation is [350 650]ms after the R peak, but three different topography, each plotting the average recorded voltage amplitude, are showed: the first focused on the [350 480]ms interval, the second in the [480 650]ms one and the third ranging in the [50 480]ms slot. The significant one is stated to be the first, showing a higher HER in the parieto-occipital regions.

- In [10] the subjects are required to count their hearbeats. The time window chosen for the HEP evaluation is [250 350]ms after the R peak. The topography shows the average recorded voltage amplitude in such time slot and the higher values are located in central and fronto-central electrode positions.

Then it is easy to see that the scenario is highly confused, with another important lack in consistency that must be observed: there is not any standard neither in the quantity showed in the topography, since someone report the average recorded voltage, others the average difference between the voltage recorded during two different tasks or even a correlation between a cortical voltage and a heart state.

Chapter 2

Materials and Methods

2.1 Partecipants

The available set of data is formed by the MEG recordings of 20 people partecipating in a study developed at the Brain and Psychological Sciences Research Center (BPsyC) of the Swinburne University of Technology. The aim of the study was to establish the difference in the evoked response to particular visual stimuli between healthy subjects versus ones affected by the General Anxiety Disorder (GAD), an anxiety disorder that is characterized by excessive, uncontrollable and often irrational worry, that is, apprehensive expectation about events or activities. The details of the subjects are listed in the following table:

ID	Status	Gender	Age	Handedness
1	GAD	F	30	Right
2	CTRL	F	22	Left
3	GAD	M	26	Right
4	GAD	M	40	Right
5	GAD	F	39	Right
6	CTRL	M	24	Right
7	GAD	F	26	Right
8	CTRL	F	26	Right
9	CTRL	M	39	Right
10	CTRL	F	32	Right
11	GAD	F	25	Right
12	GAD	F	24	Right
13	CTRL	F	31	Right
16	GAD	M	25	Right
17	CTRL	M	36	Right
19	CTRL	M	27	Right
21	GAD	F	30	Right
22	CTRL	F	22	Right
24	GAD	M	21	Right
25	GAD	M	37	Right

The purpose of this project is to study the HER, a physiological feedback which is reasonable to consider uncorrelated to any mental disorder involving the anxiety:

in fact, even if it could be argued that anxiety might affect the heartbeat rate, in terms of the HER it would just mean that a higher number of response signals will be present. Therefore, for the scope of this research, no distinction between the mental health of the subjects will be considered.

2.2 Paradigms

The analysed data belongs to the two resting conditions recording of the GAD study: that is the subjects were simply demanded to relax and keep, respectively, the eyes closed and open for a duration of about 5 minutes each. In this time interval, the MEG and the ECG were recorded at the same time. In our scenario, the heartbeats are the target stimuli whose response has to be evaluated, therefore the ECG will provide the time indices of such stimuli, which concur with the R peaks in the ECG waveform.
However, since the ECG is the key for the stimuli identification, any error in its recording will affect the whole data set for a certain subject. Because of this, the data of 2 subjects in the Eyes Closed condition and of 4 in Eyes Open one had to be discarded: in fact, likely due to misplacement of the electrodes during the recording, the ECG traces resulted unsuitable for a correct detection of the R peaks.

2.3 On-line acquisition system

Continuous MEG signals were collected using a whole-head MEG system with 102 magnetometers and 204 planar gradiometers (Elekta Neuromag TRIUX MEG system) at a sampling rate of 1,000 Hz.
The data were then stored for the off-line processing and analysis, which is basically the core of this work. However, the actual data used in this analysis were previuously filtered with MaxFilter to remove the main non-cortical noise components.

2.4 Software

All the analysis was carried out using MatLab and MatLab-based toolbox: in particular, the FieldTrip [12] toolbox was widely exploited in the all analysis, both in the sensor and source space. The SPM toolbox [13] robust average implementation was used in the averaging process. Finally, complementary customised scripts were then used for various purposes.

Chapter 3

Analysis scope and model

3.1 Approach

As discussed in the first chapter, there is a remarkable lack of consistency in the literature about the HER localization and timing. This situation is likely due to the approach generally adopted: in fact, every study compares the HER between two specific experimental conditions, which are obviously different in every work. Basically, the HER is assumed to exist, which is a reasonable assumption because of the physiological links between brain and heart, and it is evaluated in specific situations to infer some kind of physiological or medical conclusion.
On the contray, the approach adopted here is slightly different: in fact the aim of this work is to evaluate the "pure" HEF, that is comparing the supposed HER against a null baseline. So, each condition is compared against a null version of itself and this can be achieved through a different segmentation of the data.
Thus, the basic approach is to segment the raw data in two different ways: one provides segments (trials) locked to the R peaks of the ECG, while the other creates trials unlocked to any stimulus.

3.1.1 Scenario

Considering a single subject s, the raw data is the continuous signal recorded by the different sensors, then such data can be stored in a matrix where each row represents a sensor (channel) and each column is the sample recorded by the sensor in that time index. Thus, the matrix will have $f_s \cdot L$ columns, where f_s is the sampling frequency and L is the time length of the considered condition for the subject s. On the other hand, rows are basically the ECG channel plus the MEG channels (magnetometers and gradiometers).
Now, the aim of the segmentation process is to create equal length trials which can then be averaged to improve the SNR (since the noise is AWGN). So, the segmentation process works as follows:

QRS locked trials: the $t = 0$ of each segment is set on the R peak of the QRS complex, then a pre and a post stimulus time lengths are selected.

Unlocked trials: here the raw data is simply segmented into fixed length trials unlocked to any stimulus; these trials will provide the desired baseline.

This process is done for both the ECG and the MEG channels, since all of them need an improvement of the SNR. Then, after the two different segmentations, we have:

- $q_m(t)$: the MEG (magnetometers/gradiometers) QRS-locked signal, with length L_q.
- $ECG(t)$: the QRS-locked signal of the electrocardiogram recording, with length L_{ECG}.
- $b_m(t)$: the MEG baseline signal (unlocked segment), with length L_b.
- $b_{ECG}(t)$: the ECG baseline signal (unlocked segment), with length $L_{b_{ECG}}$.

Remark:

- $L_q = L_{ECG} \triangleq L_{QRS}$
- $L_b = L_{b_{ECG}} \triangleq L_{BL}$
- $L_{QRS} \neq L_{BL}$

The chosen values for L_{QRS} and L_{BL} will be detailed in the next chapter.

3.1.2 Observation about the baseline choice

The most commonly adopted baseline is a time window belonging to the pre-stimulus interval, whose mean value is then taken as the 0 reference; however such approach is unfeasible in our scenario, since it would cancel out what we are looking for.
First of all, it has been well established that the HER has to be evaluated in the time window where the heart is in a resting condition, that is its electrical activity is null, and such window occurs after the T wave, resulting roughly in the time interval of $[350\ 650]ms$ after the R peak (which is the $t = 0$ reference). Now, a baseline to be reasonable must range in a resting condition, that is spanning a temporal interval where no interesting phenomenon is likely to occur. Therefore, if a pre-stimulus interval were chosen, this should be a window $W_{pre} = \{t|\ t_{min} < t < t_{max},\ t_{max} < -200ms\}$ since at $t \simeq -200ms$ the P wave starts; furthermore, to have a good estimate of the mean value the condition $W_{pre} \geq 200ms$ is necessary.
Now, the QRS-locked trials are obtained "cutting" the continuous data into segments centered on the time index of the the R peak, t_R. Assuming to choose a pre-stimulus interval of $400ms$, to get a "classic" baseline, and a post-stimulus of $650ms$, to span the whole HER evaluation window, and assuming an average heart rate of $70bpm \Rightarrow T_{HB} = 875ms$, for the beats i and $i+1$ we have the following situation:

$$\begin{cases} t_R^{(i)} = 0ms,\ W^{(i)} = [-400\ 650]ms \\ t_R^{(i+1)} = 875ms,\ W^{(i+1)} = [475\ 1525]ms \end{cases} \Rightarrow W_{HER}^{(i)} \cap W_{pre}^{(i+1)} \neq \emptyset. \qquad (3.1)$$

Since it is reasonable to assume $|HER^{(i)}| \simeq |HER^{(i+1)}|$, from (3.1) it can be seen that the HER is evaluated through a comparison against itself, which will always provide a null result. Furthermore, the higher is the heart rate the higher is the

overlap, worsening the situation.
That is why a different choice of the baseline is necessary and the adopted one is justified by the mathematical model detailed below.

3.2 Mathematical model

The data considered is a set of signals which are stochastic processes, so a suitable model has to been identified in order to undertake a valid analysis. However, an important observation is that the MEG (and EEG) data are normally distributed.

3.2.1 The ECG signal

The recorded ECG trial k can be modeled as:

$$ECG^{(k)}(t) = HB(t) + e(t), \tag{3.2}$$

where:

- $HB(t)$: pure cardiac activity.
- $ECG(t)$: recorded signal representing the cardiac activity.
- $e(t) \sim \mathcal{N}(0, \sigma^2)$: recording error.

The assumption that the noise component is just AWGN is well verified in the ECG, EEG and MEG recording scenarios.

About the baseline, we know that:

$$b_{ECG}(t) \sim \mathcal{N}(\beta_{ECG},\ \sigma^2_{ECG}) \tag{3.3}$$

Furthermore, the HER evaluation window is defined as a time interval where the heart is in a resting condition, that is the amplitude of the recorded signal is settled on the reference (baseline) value:

$$W_{HER} \triangleq \{t|\ ECG(t) \simeq b_{ECG}(t)\} \tag{3.4}$$

Now, if the available number of trials is sufficiently large to make the law of large number hold, after the averaging process we get:

$$\begin{cases} \bar{e}(t) \simeq 0 \\ \bar{b}(t) \simeq \beta_{ECG} \end{cases} \tag{3.5}$$

From which we have:

$$\overline{ECG}(t) \simeq \beta_{ECG} \quad \forall t \in W_{HER} \tag{3.6}$$

3.2.2 MEG

The MEG channels are recording the cortical brain activity and the segmentation of the trials around the R peaks means that the target stimulus is the heart beat, which is projected on the brain through the vagus nerve. However, due to the complexity of the brain, a general on going activity is present too and in our context is a noise component as the recording noise. Thus, the model for the QRS-locked trial signal in the trial k is:

$$q_m^{(k)}(t) = \mathscr{P}(HB(t)) + h(t) + n(t) + e(t), \tag{3.7}$$

where:

- $\mathscr{P}(HB(t))$: projection of the cardiac activity in the brain.
- $h(t)$: heartbeat evoked field (HEF).
- $n(t)$: other on going brain activity.
- $e(t)$: the recording AWGN.

Observation: $\mathscr{P}(HB(t))$ is not a cardiac artifact, that is the field generated by the electrical activity of the heart and recorded by the MEG, but it is a proper cortical activity which reflects the ECG trend (save for the polarity) in many area of the brain.

Then the baseline can be simply modeled as:

$$b_m^{(k)}(t) = \tilde{n}(t) + e(t) \tag{3.8}$$

where:

- $\tilde{n}(t)$: unlocked brain activity; it includes $\mathscr{P}(HB(t))$ and $h(t)$ samples.
- $e(t)$: the recording AWGN.

The unlocked brain activity can be formally modeled as:

$$\tilde{n}(t) = p_1\mathscr{P}(HB(t)) + p_2 h(t) + n(t) + e(t), \tag{3.9}$$

where the p_i indicate the probability that the samples at time t belongs either to $\mathscr{P}(HB(t))$ or to $h(t)$; to be noted that $n(t)$ and $e(t)$ are background signals which superimpose on the other components at each time sample. The p_i are time-dependent distributions, but their exact formulation is not relevant in the scope of this analysis.

Now, the presence of $h(t)$ samples in the baseline trials does not invalidate the choice of such baseline: in fact, due to the limited duration of the HEF and an expected lower magnitude of its amplitude compared to $\mathscr{P}(HB(t))$, such samples are actually negligible in the average trend. Thus, since it holds:

$$b_m^{(k)}(t) \sim \mathcal{N}(\beta_m,\ \sigma_m^2), \tag{3.10}$$

considering the averaged signals, we have:

$$\mathscr{P}(HB(t)) + n(t) = \beta_m \quad \forall t \in W_{HER} \tag{3.11}$$

Therefore the HEF can be defined as:

$$h(t) \triangleq q(t) - b(t) \quad \forall t \in W_{HER} \tag{3.12}$$

3.3 Basic structure of the analysis

The MEG (and ECG) data, as commented before, are stochastic signals with an undesired noise component too. Therefore the data analysis has to include suitable procedure to handle these two problems, in order to legitimate any statements about the results.
From the mathematical model, the noise cancelation appears to be easily solvable through an averaging process; on the other hand, the statistical tool required to handle the random trend of the data is more sophisticated and it will be detailed in the next chapter.
However, the very basic structure of the analysis is organized as follows:

Single Subject analysis: preliminary study on a single subject basis to establish if the HEF is an actual common phenomenon and in case to evaluate its features (scalp area interested and respective time courses)

Multi Subject analysis: to try to identify the scalp areas where it is most likely to observe the HEF as well as its most typical time trend. Furthermore, undertaking the evaluation of cross-subjects characteristics which might correlates with the HEF.

An important observation is that for the main purpose of this work, that is the evaluation of the "pure" HEF, no distinction between GAD and control subjects has to be done: in fact the GAD is a mental disorder which is not correlated with any cardiac dysfunction, so it is reasonable to assume that the pure cardiac feedback to the brain behaves similar ways and the mathematical validity is not affected.
On the other hand, two datasets will be considered separately: the Eyes Closed and the Eyes Open conditions. These are both resting conditions, since the aim of this work is to evaluate a "pure" HEF, independent of any interfering task, and they will be treated independently, in order to be able in the end to compare the results, adopting the consistency among them as measure of resilience.

Chapter 4

The data processing protocol

The main part of the data processing is done on the single subject basis, since the first aim is to get clean data through the averaging process. Of course before averaging, some other steps are required, i.e. a band pass filtering between $1-40Hz$ to eliminate the main noise components. The adopted protocol is the following one:

1. reading the raw data with band-pass filtering between $1-40Hz$;
2. finding the R peaks in the ECG;
3. segmenting the raw data into both R-locked trials and into fixed time-length trials to get the baseline;
4. time-locked robust average of both R-locked and baseline trials;
5. cluster based permutation test between trials;
6. cluster based permutation test within subjects.

The assessment of this protocol is the result of adapting, through different tests, the most common processing protocols found in the literature to the aim of this work. For the sake of brevity, the intermediate steps that led to such protocol are not reported in this document. However, an interesting problem of this protocol will be highlighted in the next chapter, showing also the final solution.
Furthermore, the analyses exploits the magnetometers data, since these are the sensors which measure the amplitude of the magnetic field generated by the brain activity. The main steps of the protocol will be described in the following sections.

4.1 The R peaks detection

The R peaks identification in the continuous ECG signal is definitely a key step in this analysis, since it will provide the time indices of the target stimulus in the MEG data. Thus, the threshold-independent technique developed by [14] was adopted: such algorithm is based on the Dynamic Plosion Index (DPI) and it showed to be effective against the fluctuations that might occur in the ECG recording, with drastic effects on threshold-based detection algorithm. A MatLab implementation of the DPI method can be found at *http://mile.ee.iisc.ernet.in/QRS/dpi_qrs.m.*

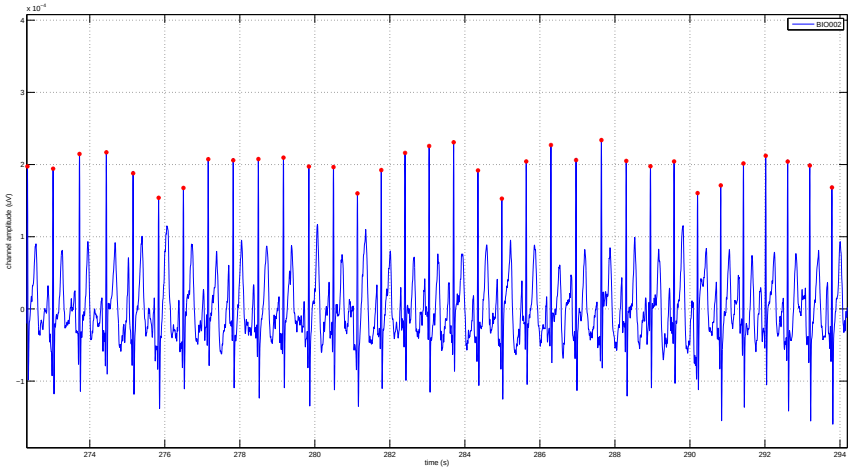

Figure 4.1: Effectiveness of the detection with DPI.

4.2 The data segmentation

The aim of segmenting the raw data is to obtain the target trials for the HEF evaluation and the baseline ones in order to perform a significant comparison.
The target trials are obtained segmenting the raw data around the time indices of the R peaks in the ECG: basically the R peak is the target stimulus in this analysis, so it represents the $t = 0$ in the trial time axis. Then, a post-stimulus interval of $600ms$ is selected, since in the literature the established window for the HER evaluation spans the $[350\ 600]ms$ interval after the R wave; furthermore, also a pre-stimulus of $500ms$ is selected, in order to have a better picture of the signal time trend.
The process to get the baseline trials is quite trivial, since it is just a segementation of the raw signal in fixed length intervals of $600ms$; this value has been chosen as the best trade-off between having a baseline spanning at least the whole post-stimulus interval and the SNR of such signal, that is the averaged baseline has to be as "flat" as possible.
For each subject s, the number of trials obtained in the QRS-locked and baseline condition is different because:

- the heart rate varies among people, so every subject has a different number of stimuli (effect on the amount of the QRS-locked trials);
- the recording length is not exactly the same for every subject (effect on the amount of both type of trials) .

4.3 The robust average

The robust average is a technique to average and to suppress artifacts at the same time. It is based on the idea of estimating the distribution of the data across

trials: that is, given a sufficiently high number of trials, the distribution of each channel-time sample is estimated across the trials. Then, the outliers are defined using the mean and the distance from the mean; in particular, every sample distanced more than 3σ from the mean is labeled as outlier. Such outliers are then downweighted in the total average computation. The SPM method used in this work is an iterative procedure whose implementation is based on [15].
The robust average allows to get results resilient against artifacts, especially the "casual" ones such as eyes movements or muscular activity which are the main concern in our scenario: in fact, the electrical activity due to cardiac contractions was already rejected by the MaxFilter, therefore the only undesired components, further than the recording noise, are these spiking artifacts that are easily labeled as outliers by the robust average. However, it is also worth to observe that, due to ease of the adopted paradigm and the short recording time (since few minutes are enough to get hundreds of target and baseline trials), the amount of such artifacts is actually small and handable by a normal averaging technique.

4.4 The cluster based permutation test

The significance of the difference in heartbeat-evoked responses between hits and misses was tested using the cluster-based permutation t test [16] as implemented in the FieldTrip toolbox. This procedure extracts spatiotemporal regions showing significant differences between conditions without any a priori on spatial regions nor time windows and intrinsically corrects for multiple comparisons in space and time. Briefly, individual samples whose t value exceeds a threshold $p < \alpha$ (two tailed) are clustered based on temporal and spatial adjacency. Each cluster defined in time and space by this procedure is assigned cluster-level statistics corresponding to the sum of the t values of the samples belonging to that cluster. Type 1 error (that is, the false positive) rate is controlled by evaluating the maximum cluster-level statistics under the null hypothesis: condition labels are randomly shuffled N_{iter} times to estimate the distribution of maximal cluster-level statistics obtained by chance. The two-tailed Monte-Carlo p value corresponds to the proportion of elements in the distribution of shuffled maximal cluster-level statistics that exceeds the observed maximum or minimum original cluster-level test statistics. Because this method uses maxima, it intrinsically corrects for multiple comparisons in time and space. The parameters chosen in the analysis were:

- SS analysis: time window $[350\ 595]ms$, $\alpha_{clust} = 0.01$, $\alpha_t = 0.05$, $N_{iter} = 700$.
- MS analysis: time window $[350\ 595]ms$, $\alpha_{clust} = 0.05$, $\alpha_t = 0.05$, $N_{iter} = 1000$.

Chapter 5

Results & Observations

The results evaluation is not straightforward from the processing protocol: in fact suitable kinds of visualization are required in order to interpret correctly the data.
First of all, the specific time window of interested has to be identified, since it is likely that the target response actually spans a subwindow of the one considered for the statistical test. To do so, a plot somehow summarising the statistical significant time intervals is necessary.
The next step is the depiction of the topographic plot, which represents a plot of the head from an on high perspective: it consists in a circular representation of the head in which are highlighted the locations of the channels according to a specific layout depending on the device used for the recording; in this case the 102 locations of the magnetometers channels are depicted. Then the desired quantity, in a specific time interval, is plotted using a color map, providing a very clear picture of the situation. Furthermore, a desired mask can be applied, allowing to show the values of the locations defined significant.
Finally, the time course visualization of some significant channel might definitely be interesting.
Such visualizations are provided first in the single subject scenario, then in the multi-subject one; in both cases the Eyes-Closed and Eyes-Open conditions are evaluated separately.

5.1 Single subject results

In the single subject analysis the input signals are the trials of the two conditions considered, that is QRS-locked and baseline. Thus, for each subject, the trials are submitted to the statistical test to see in which channels and in which time interval it is likely to observe a real HEF; then, in order to improve the SNR and to get a concise visualization of the results, the average among the trials is evaluated and used to depict the different kinds of plot described before.

5.1.1 Time window

The aim is to visualize if the QRS-locked trials are statistically significant from the baseline ones in a common time interval among the subjects. Thus, the plot

has on the horizontal axis the time window considered for the statistical test - [350 595]ms - and on the vertical axis the subjects ID; the plotted function is:

$$f(t) = \begin{cases} k & \text{if } \exists\ m \text{ significant at time } t \\ null & \text{otherwise} \end{cases}$$

where k is the numerical value provided by the subject ID. This plot does not show any consistency in the channel significance for a certain subject, so it must be considered as a very first visualization of any time consistency among subjects.

Eyes Closed

The subject set is: $ID_{EC} = \{2; 3; 4; 5; 6; 7; 8; 9; 10; 12; 13; 16; 17; 21; 22; 25\}$

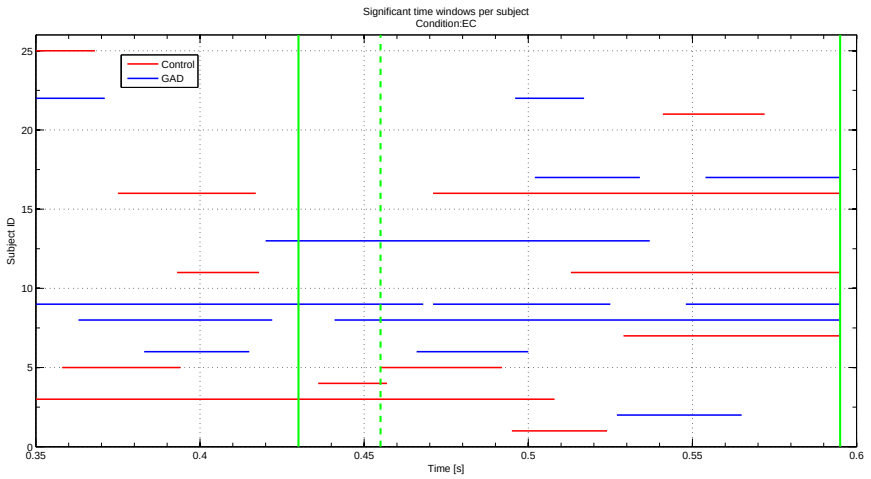

Figure 5.1: Significant time windows for the EC data.

The vertical green lines highlight the time window identified as significant to evaluate the HEF -[430 595]ms-, that is the time interval where the highest number of subject shows the highest probability to see an actual HEF. The dashed line depicts the lower bound of the time window considered in [2] (that is, [455 595]ms), which was our first reference.

Eyes Open

Here, the subject set is: $ID_{EO} = \{1; 2; 3; 4; 5; 6; 7; 8; 9; 10; 11; 12; 13; 16; 17; 21; 22; 25\}$

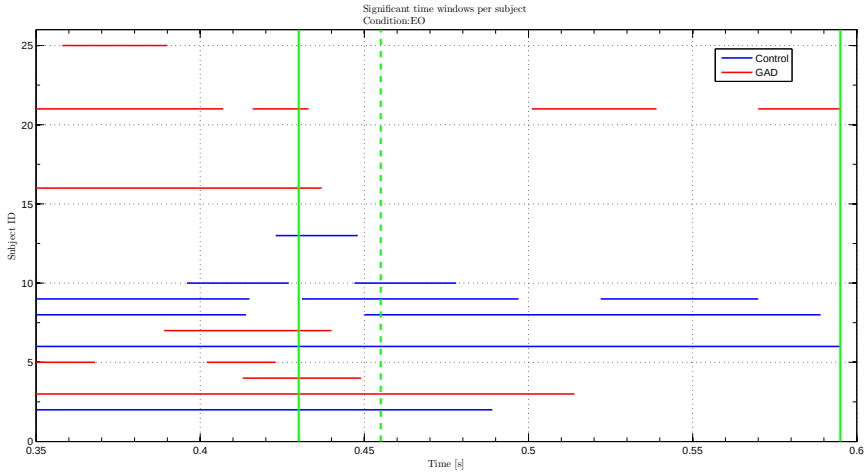

Figure 5.2: Significant time windows for the EO data.

It can be observed that in the EO case the time window is different than in the previous situation, spanning roughly from 350 to 500ms.

5.1.2 Topography

The quantity depicted in the following topographic plots is:

$$f(m) = \overline{h}_m = \overline{q}_m - \overline{b}_m = \left(\frac{1}{|W_{HER}|} \sum_{t=t_{beg}}^{t_{end}} q_m(t) \right) - \left(\frac{1}{|W_{HER}|} \sum_{t=t_{beg}}^{t_{end}} b_m(t) \right),$$

that is, the amplitude of the HEF in the location m, averaged in the time window considered, whose number of time samples is $|W_{HER}|$. We recall that $q_m(t)$ and $b_m(t)$ represent respectively the QRS-locked and the baseline signal averaged among the trials.
Furthermore, a statistical mask is applied: that is, just the locations labeled as significant by the statistical test are shown on the plot.

Eyes Closed

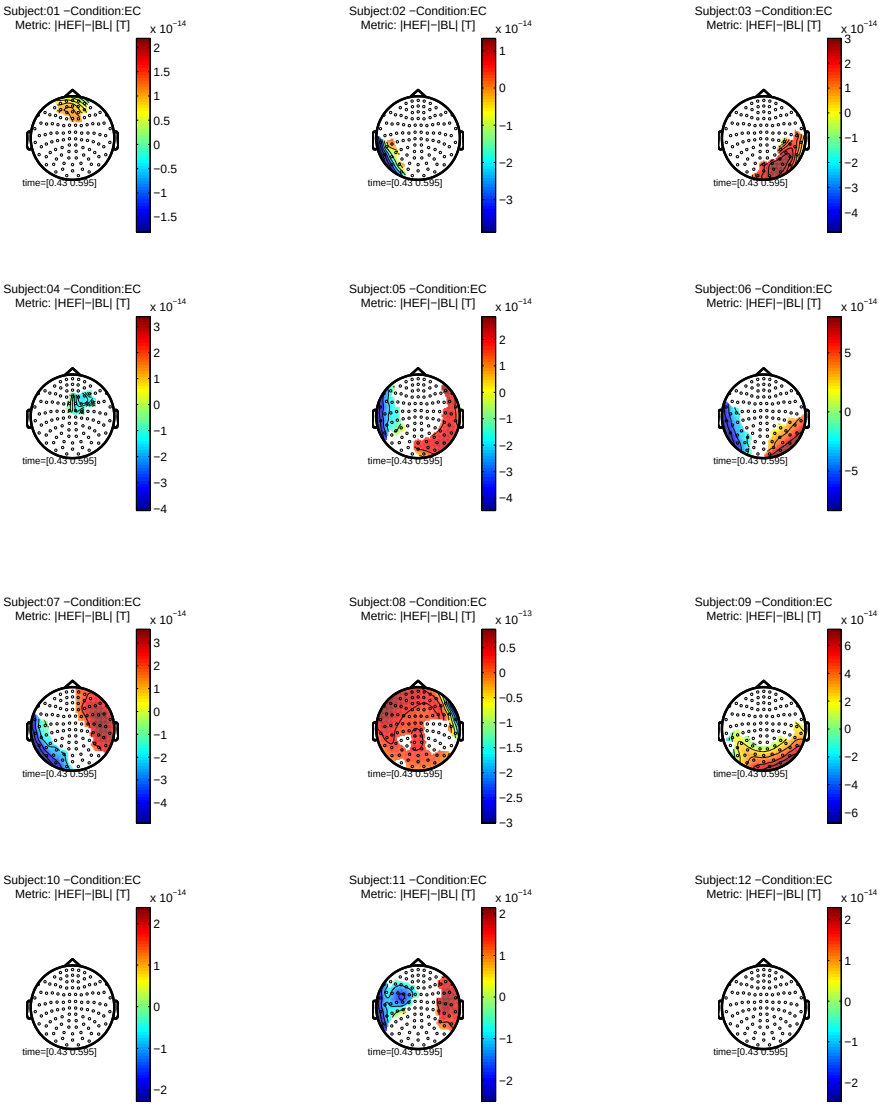
Subject:01 −Condition:EC
Metric: |HEF|−|BL| [T]
x 10^−14
time=[0.43 0.595]
Subject:02 −Condition:EC
Metric: |HEF|−|BL| [T]
x 10^−14
time=[0.43 0.595]
Subject:03 −Condition:EC
Metric: |HEF|−|BL| [T]
x 10^−14
time=[0.43 0.595]
Subject:04 −Condition:EC
Metric: |HEF|−|BL| [T]
x 10^−14
time=[0.43 0.595]
Subject:05 −Condition:EC
Metric: |HEF|−|BL| [T]
x 10^−14
time=[0.43 0.595]
Subject:06 −Condition:EC
Metric: |HEF|−|BL| [T]
x 10^−14
time=[0.43 0.595]
Subject:07 −Condition:EC
Metric: |HEF|−|BL| [T]
x 10^−14
time=[0.43 0.595]
Subject:08 −Condition:EC
Metric: |HEF|−|BL| [T]
x 10^−13
time=[0.43 0.595]
Subject:09 −Condition:EC
Metric: |HEF|−|BL| [T]
x 10^−14
time=[0.43 0.595]
Subject:10 −Condition:EC
Metric: |HEF|−|BL| [T]
x 10^−14
time=[0.43 0.595]
Subject:11 −Condition:EC
Metric: |HEF|−|BL| [T]
x 10^−14
time=[0.43 0.595]
Subject:12 −Condition:EC
Metric: |HEF|−|BL| [T]
x 10^−14
time=[0.43 0.595]

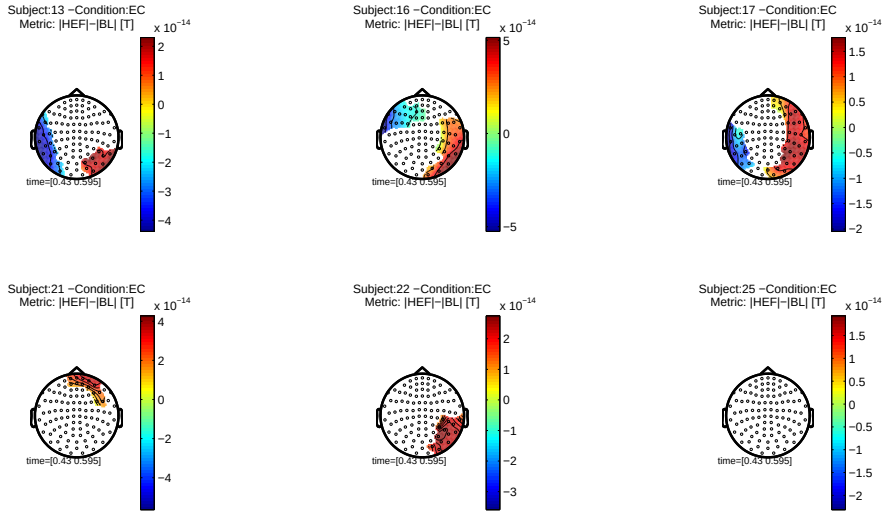

Figure 5.3: Eyes Closed topographic plots

The high variability among subject can be immediately observed. Nevertheless, a certain consistency in the right central and occipital areas is remarkable.

Below few examples of the time course of significant channels are showed for two sample subjects. The first plot depicts the ECG channel, while the others are magnetometers.

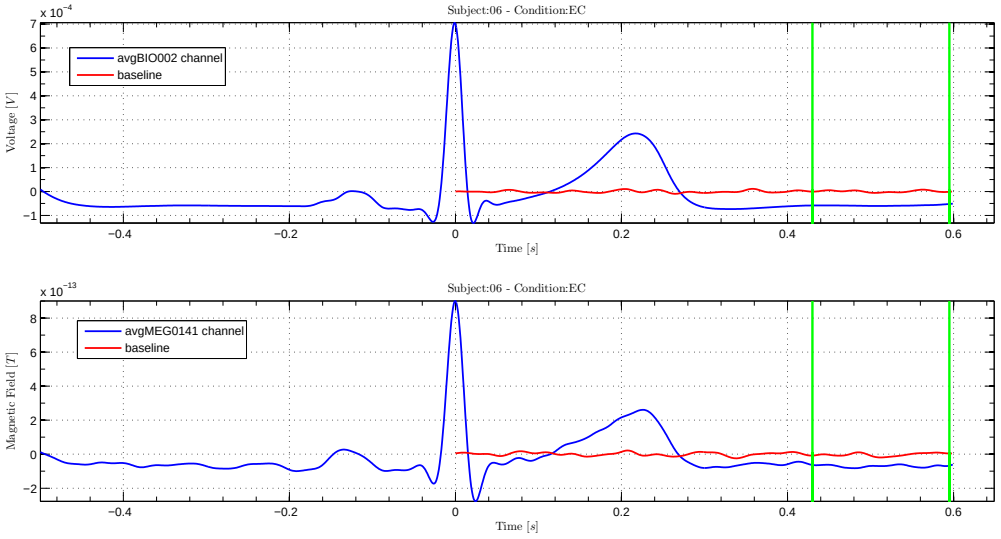

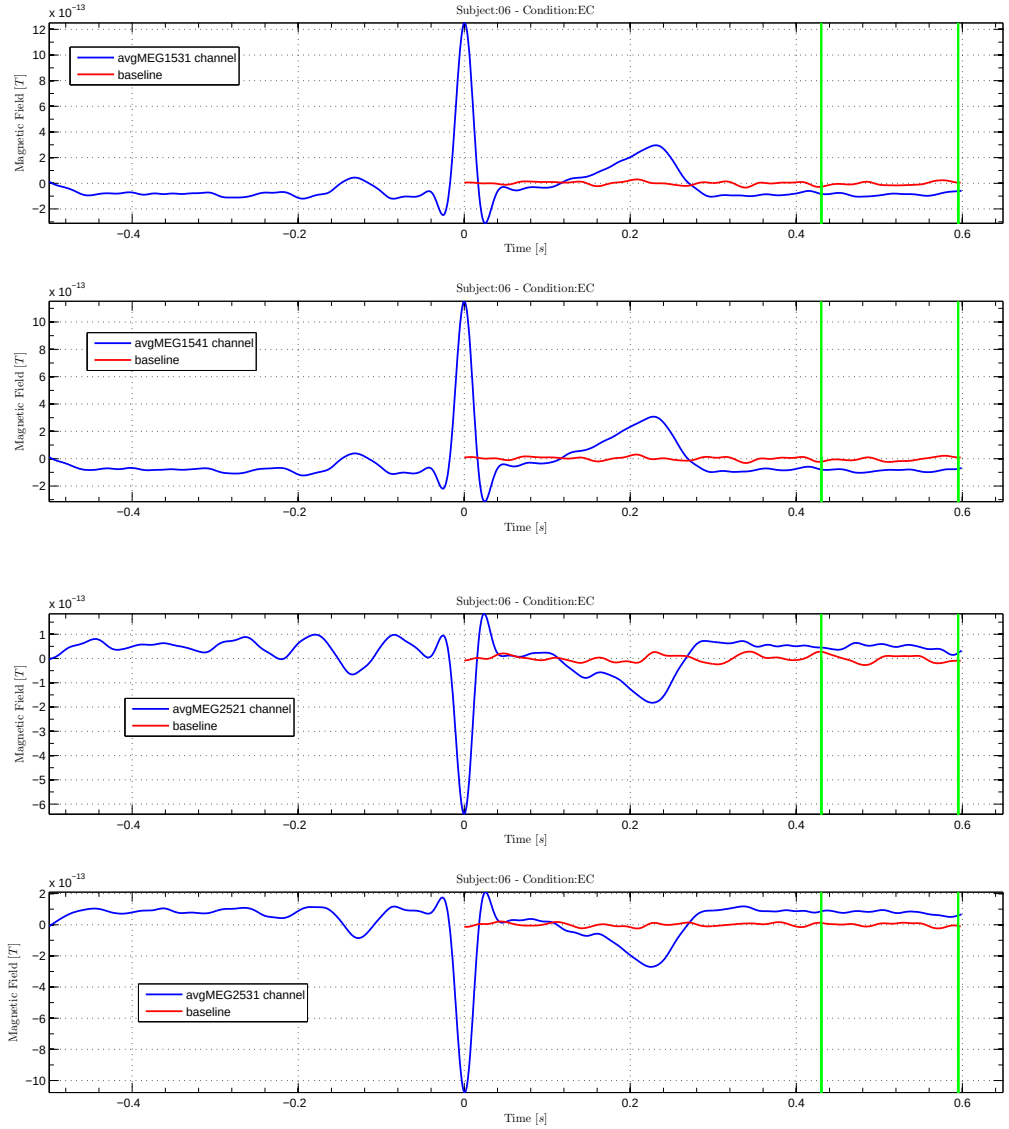
Subject:06 - Condition:EC
x 10^-13
avgMEG1531 channel
baseline
Magnetic Field [T]
Time [s]
Subject:06 - Condition:EC
x 10^-13
avgMEG1541 channel
baseline
Magnetic Field [T]
Time [s]
Subject:06 - Condition:EC
x 10^-13
avgMEG2521 channel
baseline
Magnetic Field [T]
Time [s]
Subject:06 - Condition:EC
x 10^-13
avgMEG2531 channel
baseline
Magnetic Field [T]
Time [s]

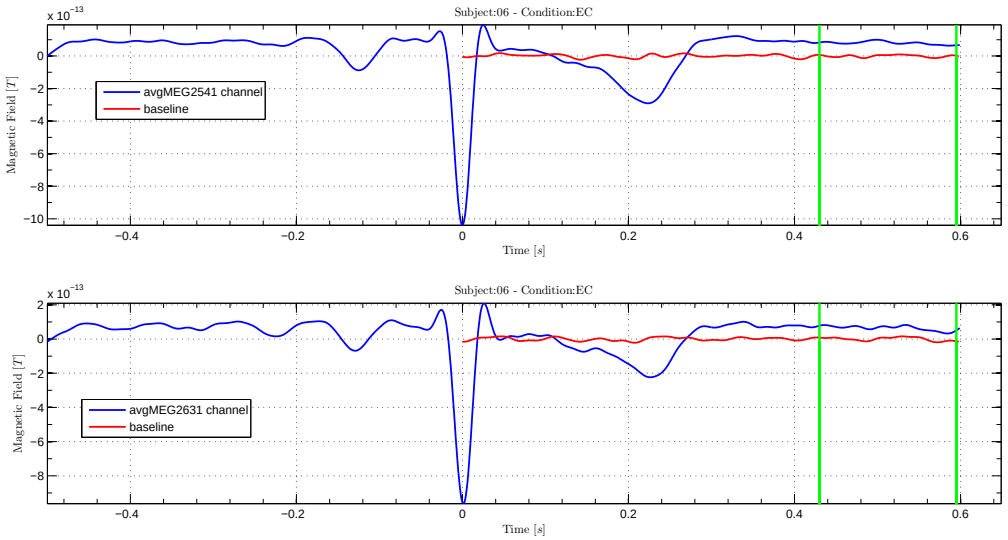

Figure 5.4: Time courses for subject 06.

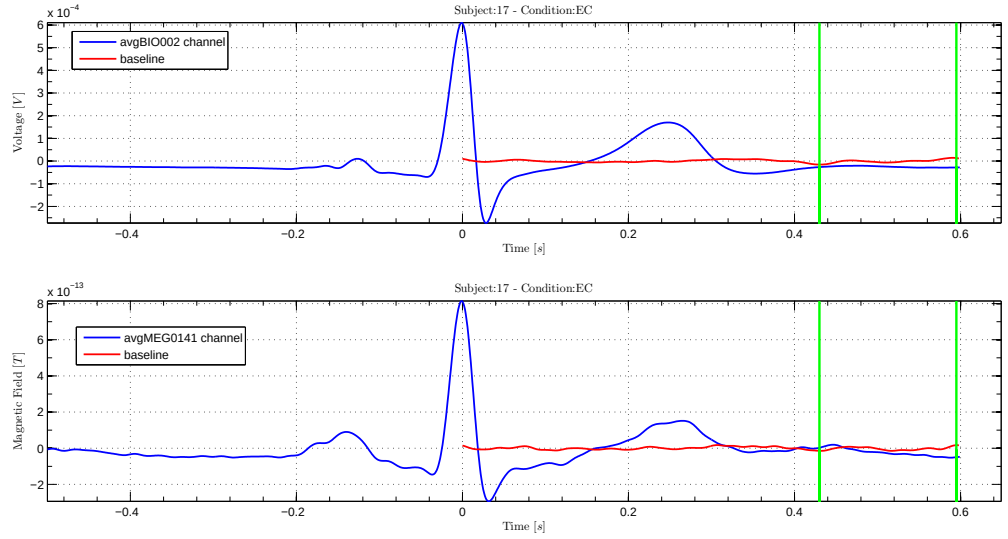

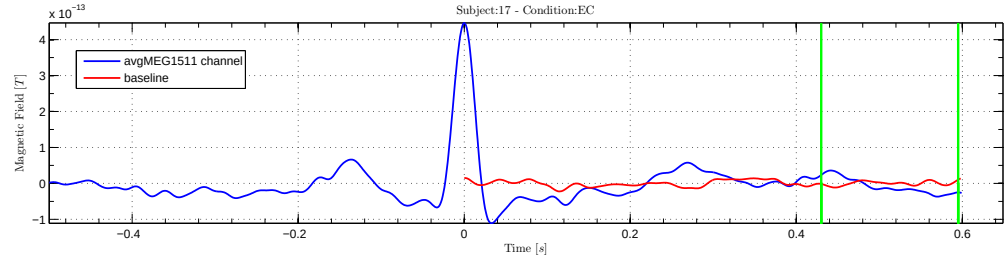
Subject:17 - Condition:EC
x 10^-13
avgMEG1511 channel
baseline
Magnetic Field [T]
Time [s]

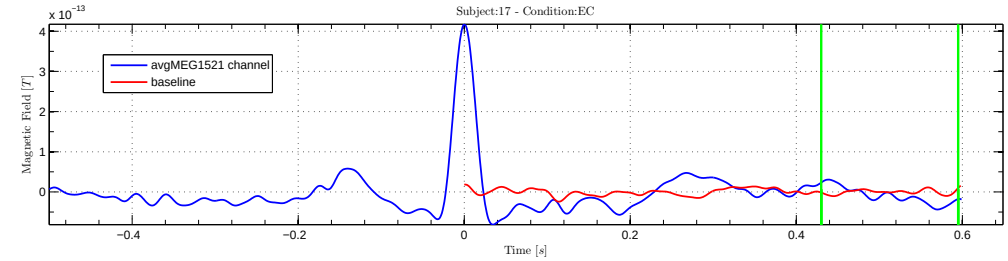
Subject:17 - Condition:EC
x 10^-13
avgMEG1521 channel
baseline
Magnetic Field [T]
Time [s]

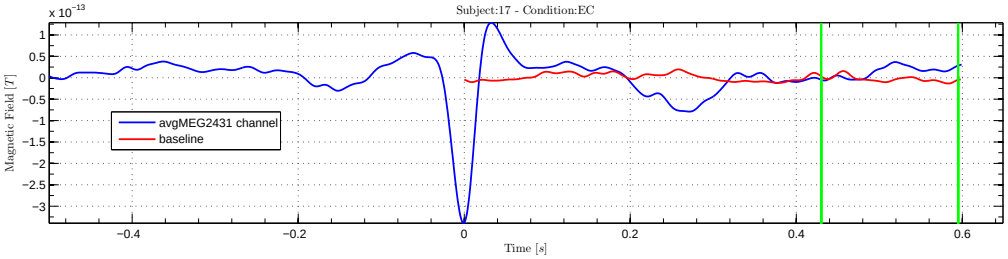
Subject:17 - Condition:EC
x 10^-13
avgMEG2431 channel
baseline
Magnetic Field [T]
Time [s]

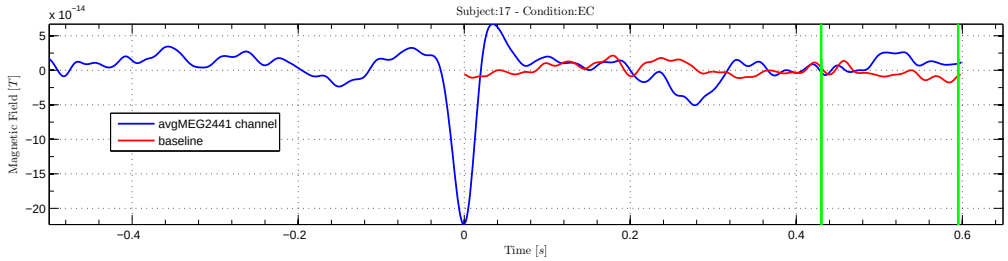
Subject:17 - Condition:EC
x 10^-14
avgMEG2441 channel
baseline
Magnetic Field [T]
Time [s]

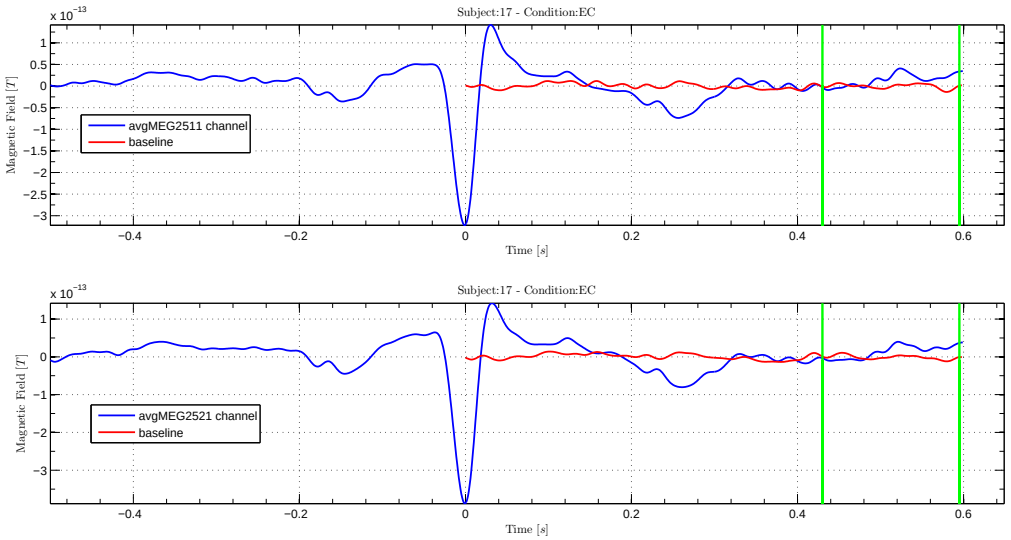

Figure 5.5: Time courses for subject 17.

Eyes Open

In the Eyes Open dataset the situation is the following:

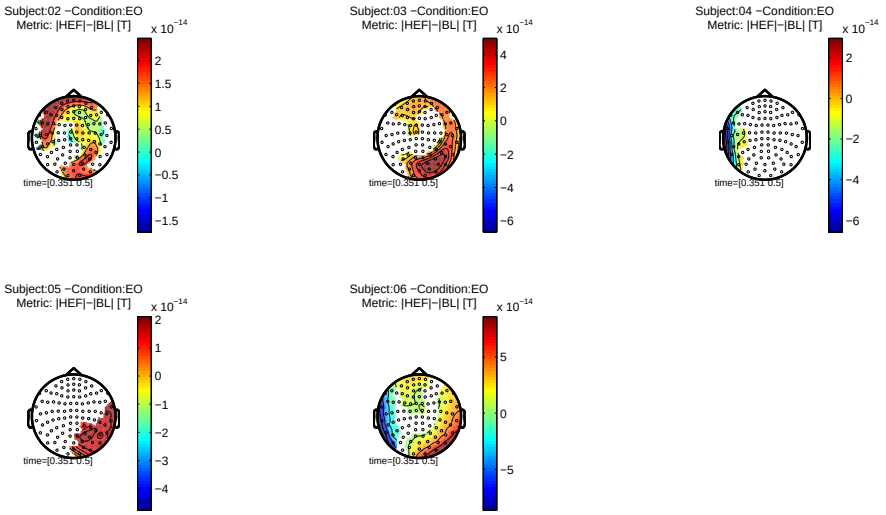

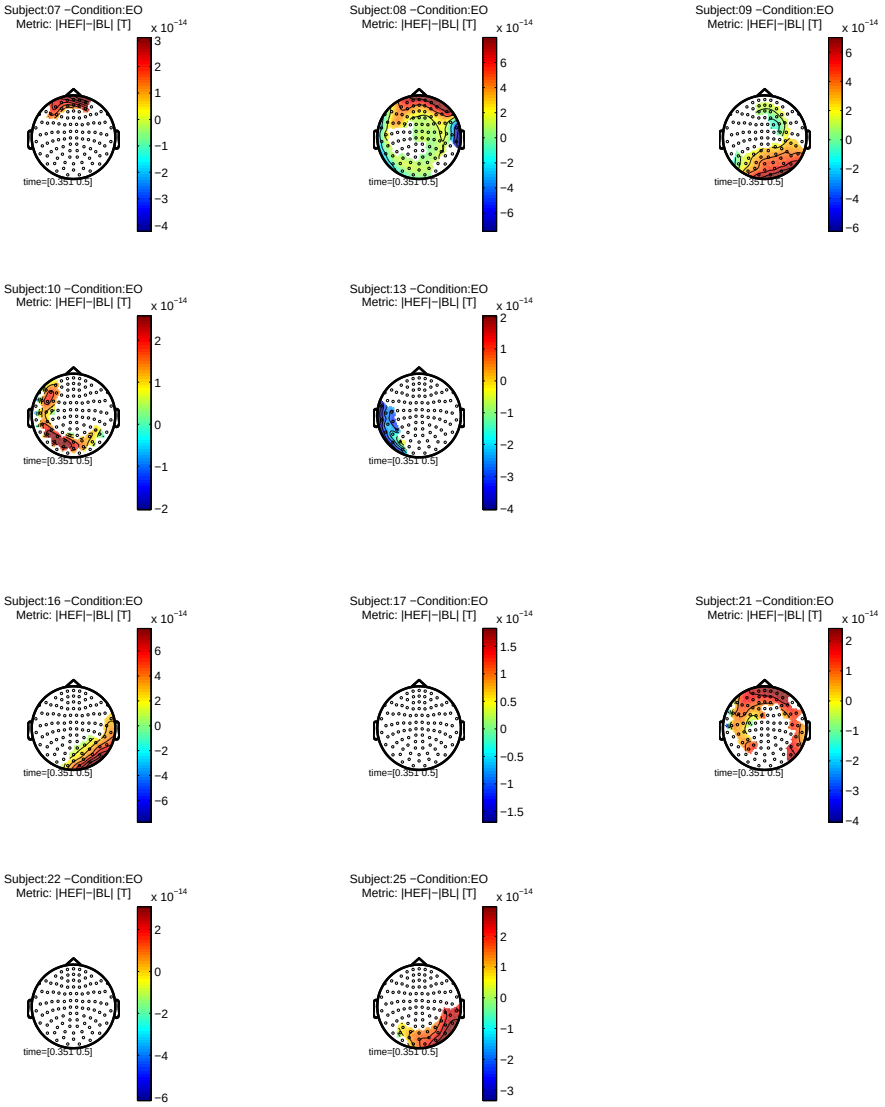

Figure 5.6: Eyes Open topographic plots

Even here the variability among subjects is quite high, however the right central and occipital areas seem to be a common pattern.

Below few examples of the time course of significant channels are showed.

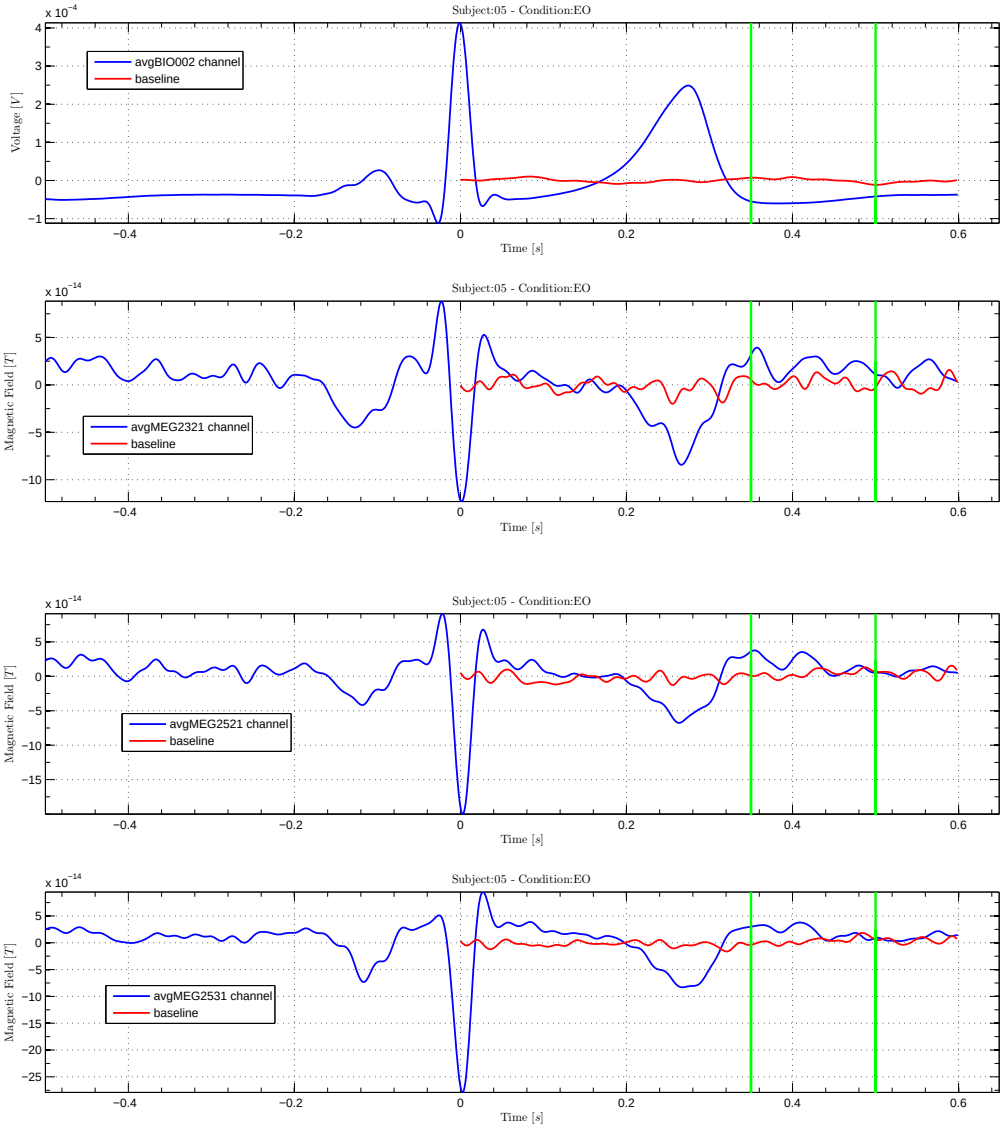
Subject:05 - Condition:EO
x 10^-4
avgBIO002 channel
baseline
Voltage [V]
Time [s]
Subject:05 - Condition:EO
x 10^-14
avgMEG2321 channel
baseline
Magnetic Field [T]
Time [s]
Subject:05 - Condition:EO
x 10^-14
avgMEG2521 channel
baseline
Magnetic Field [T]
Time [s]
Subject:05 - Condition:EO
x 10^-14
avgMEG2531 channel
baseline
Magnetic Field [T]
Time [s]

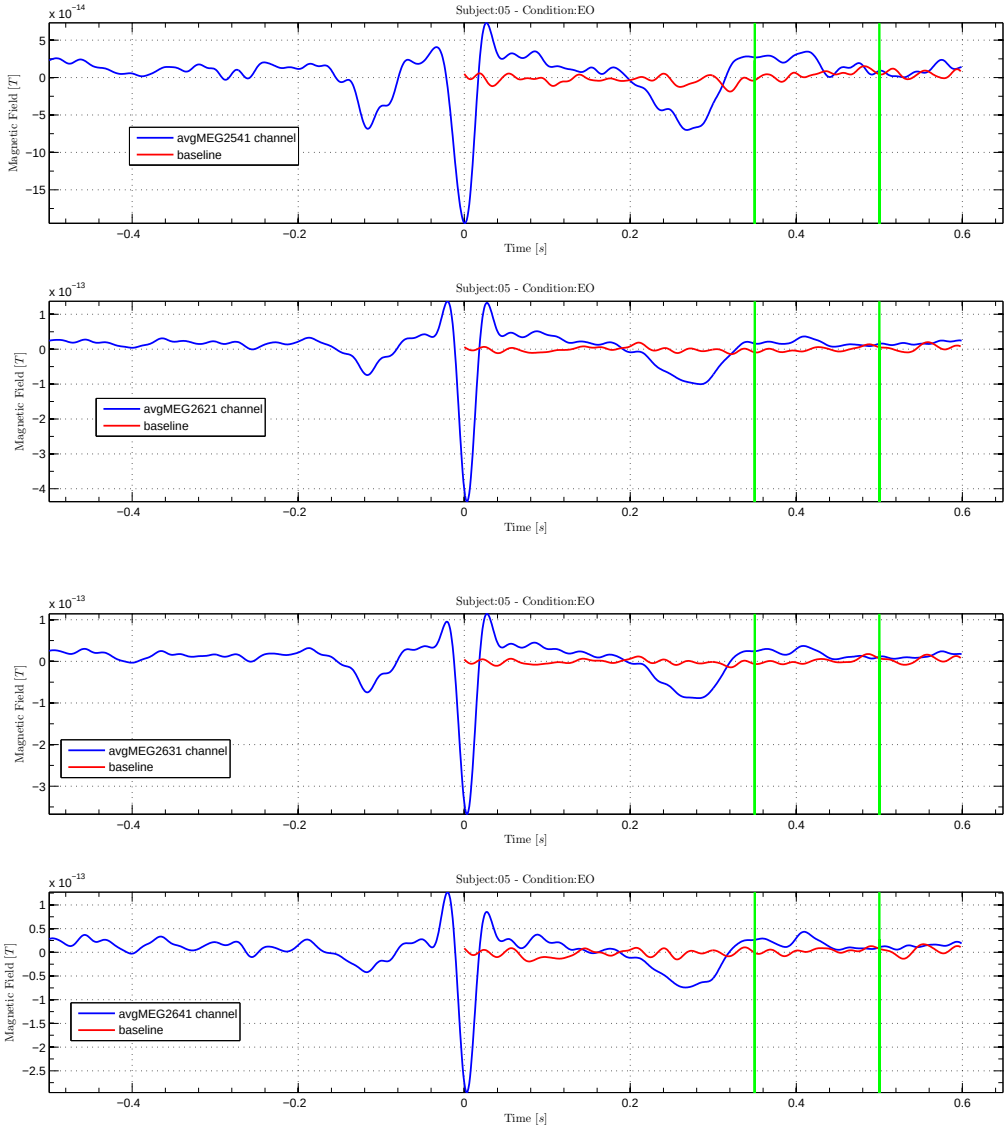

Figure 5.7: Time courses for subject 05.

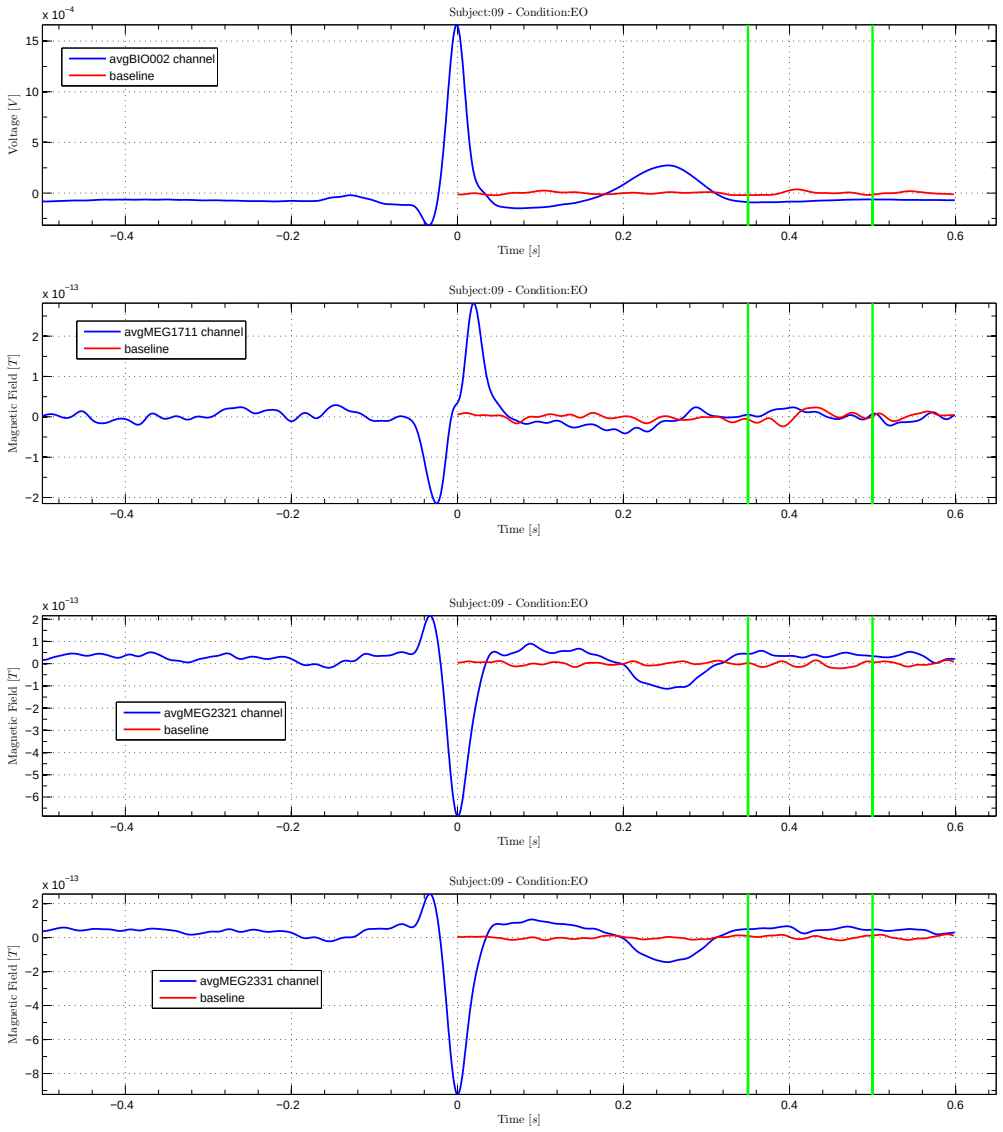
Subject:09 - Condition:EO
x 10^-4
avgBIO002 channel
baseline
Voltage [V]
Time [s]
Subject:09 - Condition:EO
x 10^-13
avgMEG1711 channel
baseline
Magnetic Field [T]
Time [s]
Subject:09 - Condition:EO
x 10^-13
avgMEG2321 channel
baseline
Magnetic Field [T]
Time [s]
Subject:09 - Condition:EO
x 10^-13
avgMEG2331 channel
baseline
Magnetic Field [T]
Time [s]

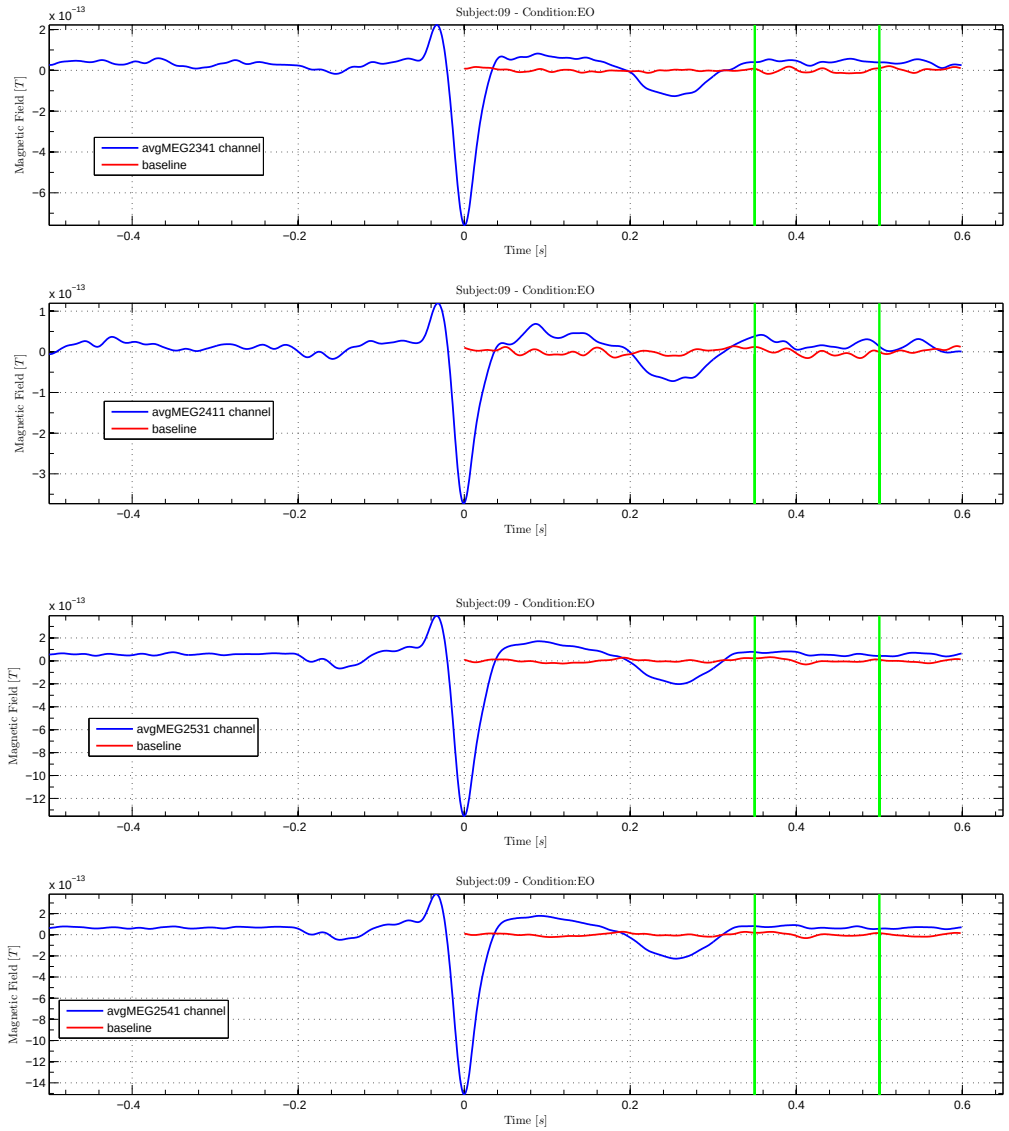

Figure 5.8: Time courses for subject 09.

5.1.3 Discussion

It has been observed that a subset of the time interval evaluated in the cluster based permutation test is a common latency among the subjects for the HEF observation. However the time windows in the Eyes Closed and Eyes Open condition are actually different.
The topography looks instead more consistent in the two cases, showing a general activation of the right central and occipital areas. Observing the time courses of the signals in such areas, it can be seen that the HEF looks more like an ongoing polarization, rather than a peak response.

5.2 Multi-subject results

In this analysis, the scope is basically a step further than the single subject study: the input signals are now the averaged QRS-locked and baseline signals of every subject, which are submitted to the statistical test to establish where and when it is more likely to observe the actual HEF. Then, the visualization is done through the grand average, that is:

$$X(t) = \frac{1}{N_s} \sum_{s=1}^{N_s} x_s(t), \tag{5.1}$$

where $x_s(t)$ is either the averaged QRS-locked or baseline signal for the subject s, and the total number of subjects considered is N_s. From now on, the grand average of the QRS-locked signal will be labeled as $Q(t)$, while the baseline one will be $B(t)$.

5.2.1 Time window

The aim is to visualize if the time intervals in which the channels show a statistically significant difference of the QRS.locked signal from the baseline. Thus, the plot has on the horizontal axis the time window considered for the statistical test - $[350\ 595]ms$ - and on the vertical axis the channels ID; the plotted function is:

$$f(t) = \begin{cases} k & \text{if } \exists\ m \text{ significant at time } t \\ null & \text{otherwise} \end{cases}$$

where k is the numerical value provided by the channel ID.

Eyes Closed

The subject set is: $ID_{EC} = \{2; 3; 4; 5; 6; 7; 8; 9; 10; 12; 13; 16; 17; 21; 22; 25\}$

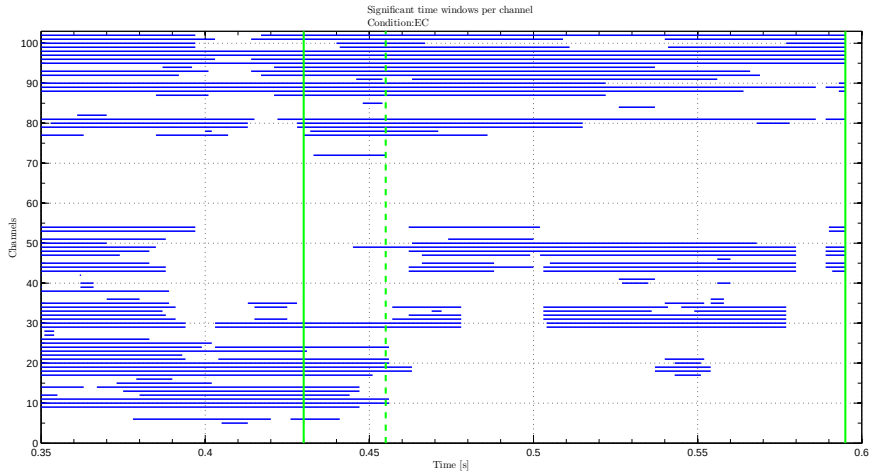

Figure 5.9: Significant time windows for the EC data.

The vertical green lines highlight the time window adopted for the EC dataset in the single subject analysis.

Eyes Open

Here, the subject set is: $ID_{EO} = \{1; 2; 3; 4; 5; 6; 7; 8; 9; 10; 11; 12; 13; 16; 17; 21; 22; 25\}$

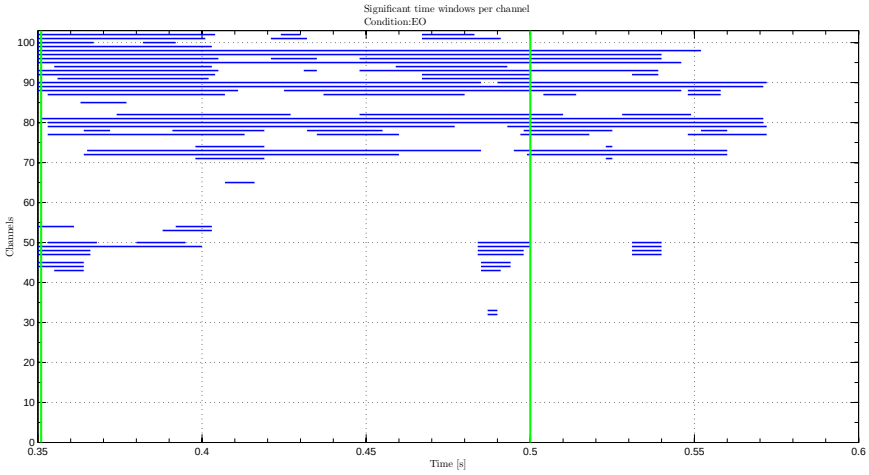

Figure 5.10: Significant time windows for the EO data.

Also here the green lines represent the latency chosen after the single subject analysis.

5.2.2 Topography

The quantity depicted in the following topographic plots is:

$$f(m) = \overline{H}_m = \overline{Q}_m - \overline{B}_m = \left(\frac{1}{|W_{HER}|} \sum_{t=t_{beg}}^{t_{end}} Q_m(t) \right) - \left(\frac{1}{|W_{HER}|} \sum_{t=t_{beg}}^{t_{end}} B_m(t) \right),$$

that is, the amplitude of the HEF in the location m, averaged in the time window considered, whose number of time samples is $|W_{HER}|$. We recall that $Q_m(t)$ and $B_m(t)$ represent respectively the QRS-locked and the baseline grand average signals. Also here, the statistical mask is applied to the plot.

Eyes Closed

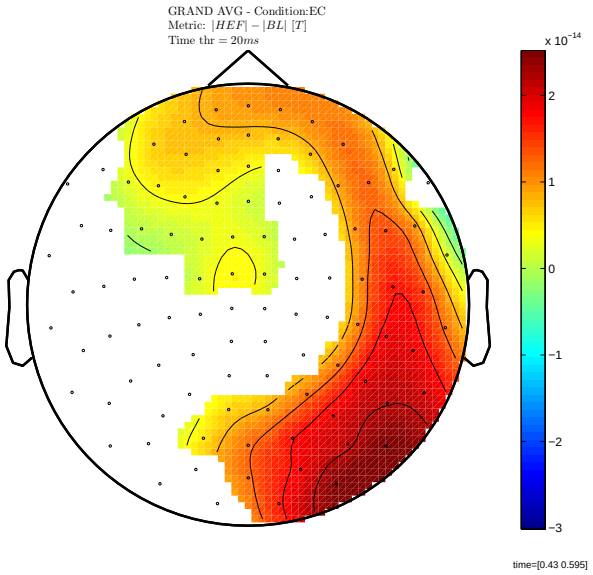

Figure 5.11: Eyes Closed topography.

The topography summarises the consistency grossly observed in the single subject analysis: that is, a HEF statistically significant from the baseline is observable in the right central and occipital areas, with an amplitude around $15 - 20fT$.

Below few examples of the time course of significant channels are showed.

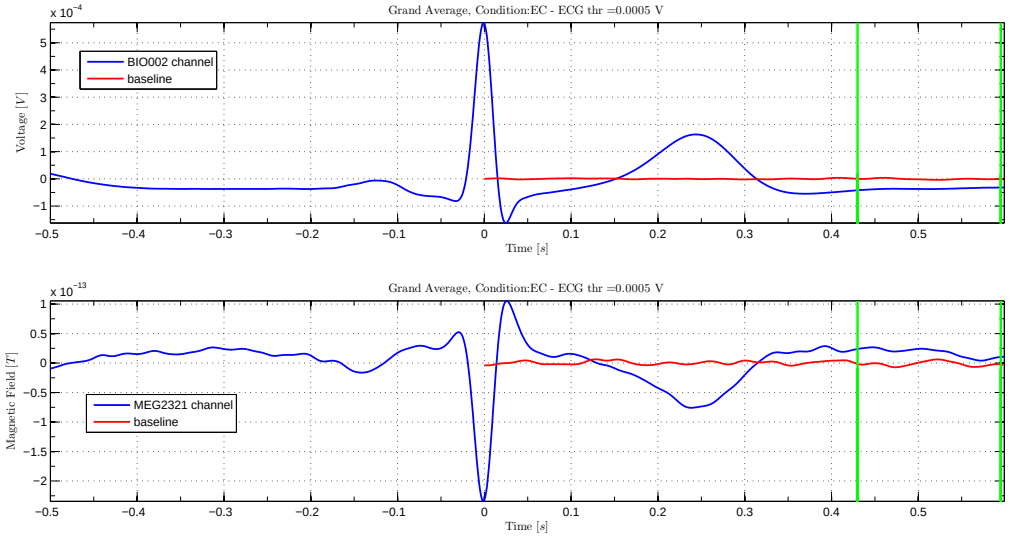

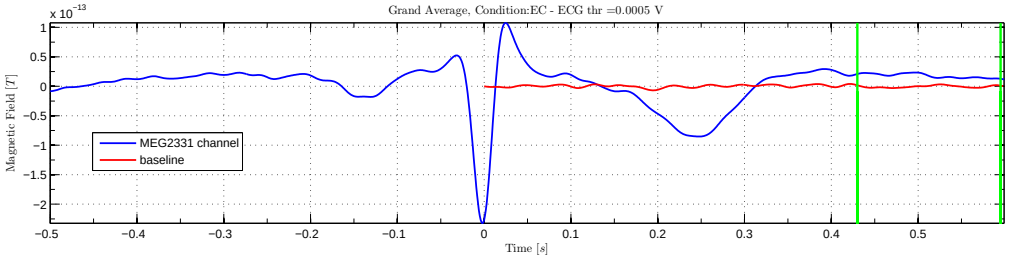
Grand Average, Condition:EC - ECG thr =0.0005 V
x 10^-13
Magnetic Field [T]
MEG2331 channel
baseline
Time [s]

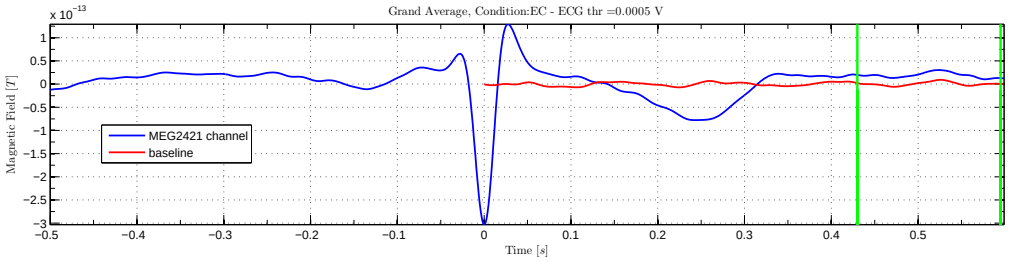
Grand Average, Condition:EC - ECG thr =0.0005 V
x 10^-13
Magnetic Field [T]
MEG2421 channel
baseline
Time [s]

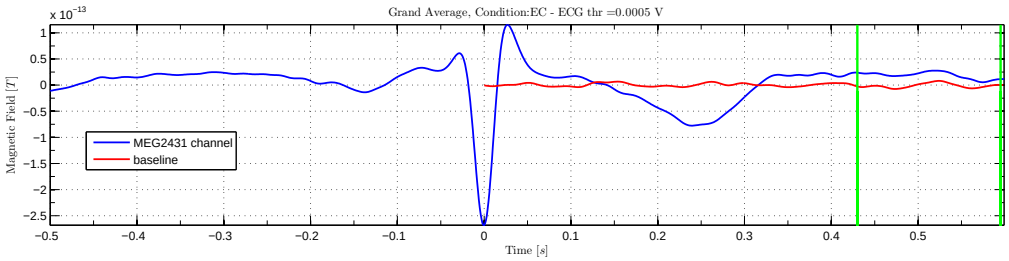
Grand Average, Condition:EC - ECG thr =0.0005 V
x 10^-13
Magnetic Field [T]
MEG2431 channel
baseline
Time [s]

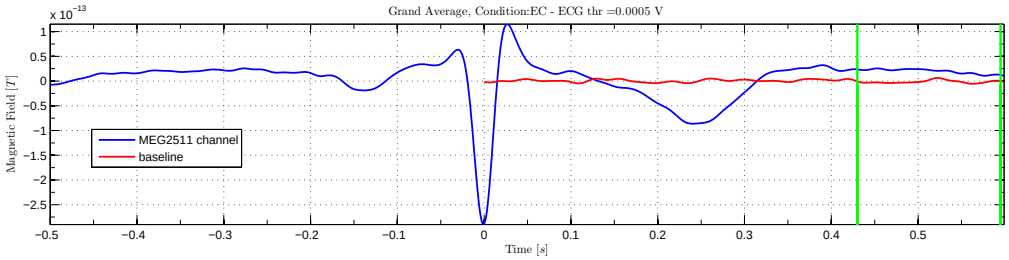
Grand Average, Condition:EC - ECG thr =0.0005 V
x 10^-13
Magnetic Field [T]
MEG2511 channel
baseline
Time [s]

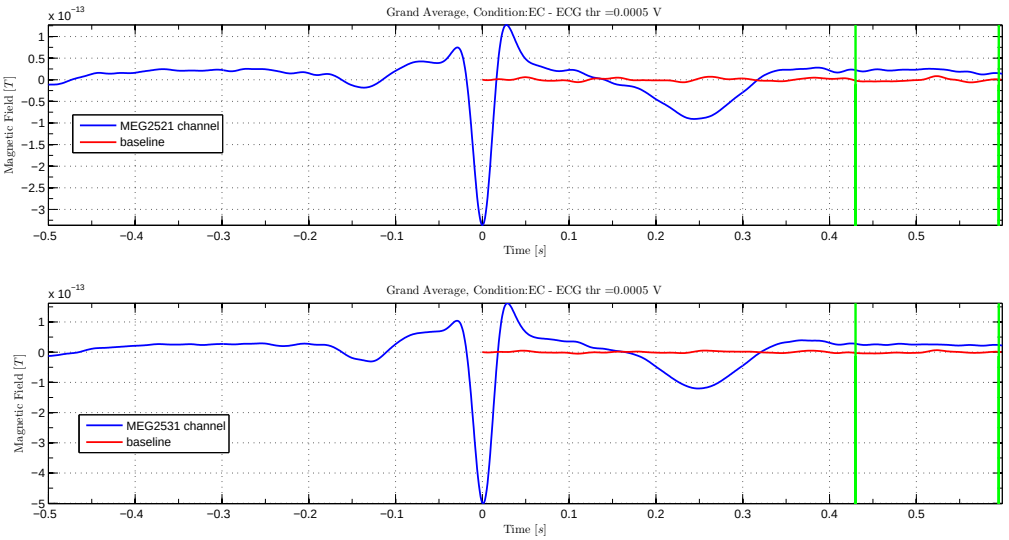

Figure 5.12: Time courses for subject.

Eyes Open

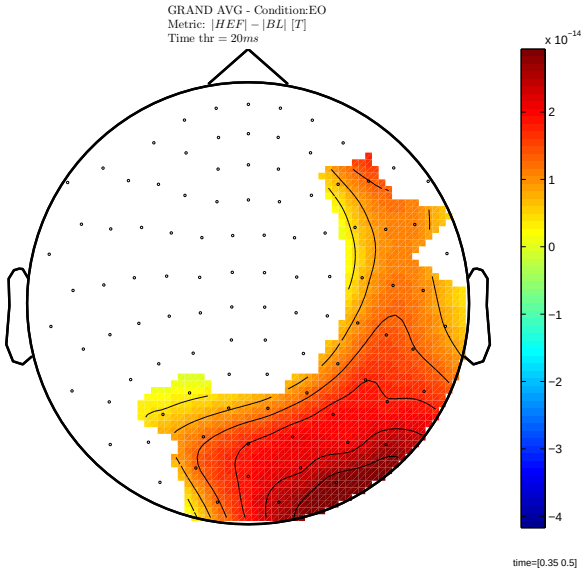

Figure 5.13: Eyes Open topography.

The consistency with the EC case is absolutely clear from this plot, showing that the right central and occipital areas are the ones where the actual HEF is likely to be observed; also the measured amplitude spans over the same range.

Below few examples of the time course of significant channels are showed.

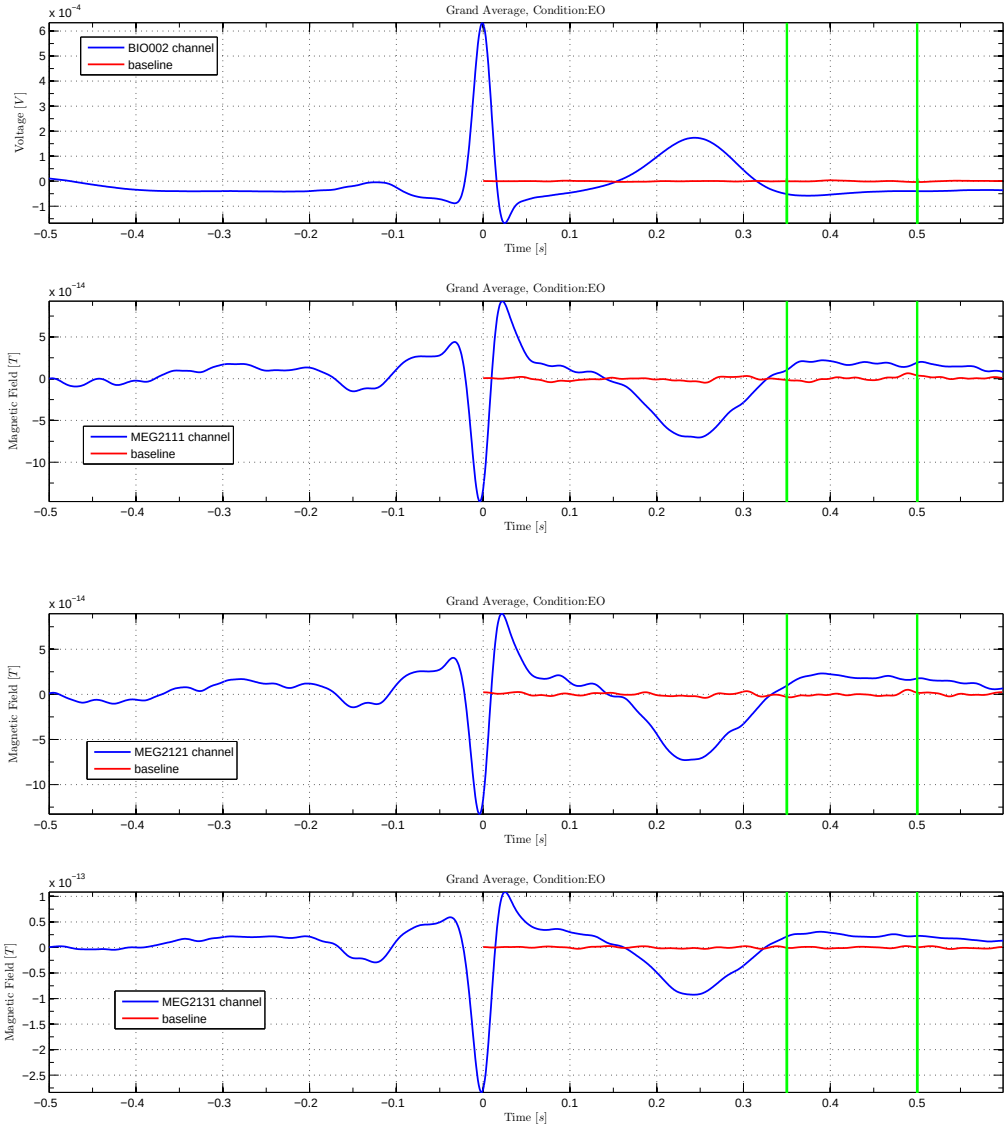
Grand Average, Condition:EO
x 10^-4
BIO002 channel
baseline
Voltage [V]
Time [s]
Grand Average, Condition:EO
x 10^-14
MEG2111 channel
baseline
Magnetic Field [T]
Time [s]
Grand Average, Condition:EO
x 10^-14
MEG2121 channel
baseline
Magnetic Field [T]
Time [s]
Grand Average, Condition:EO
x 10^-13
MEG2131 channel
baseline
Magnetic Field [T]
Time [s]

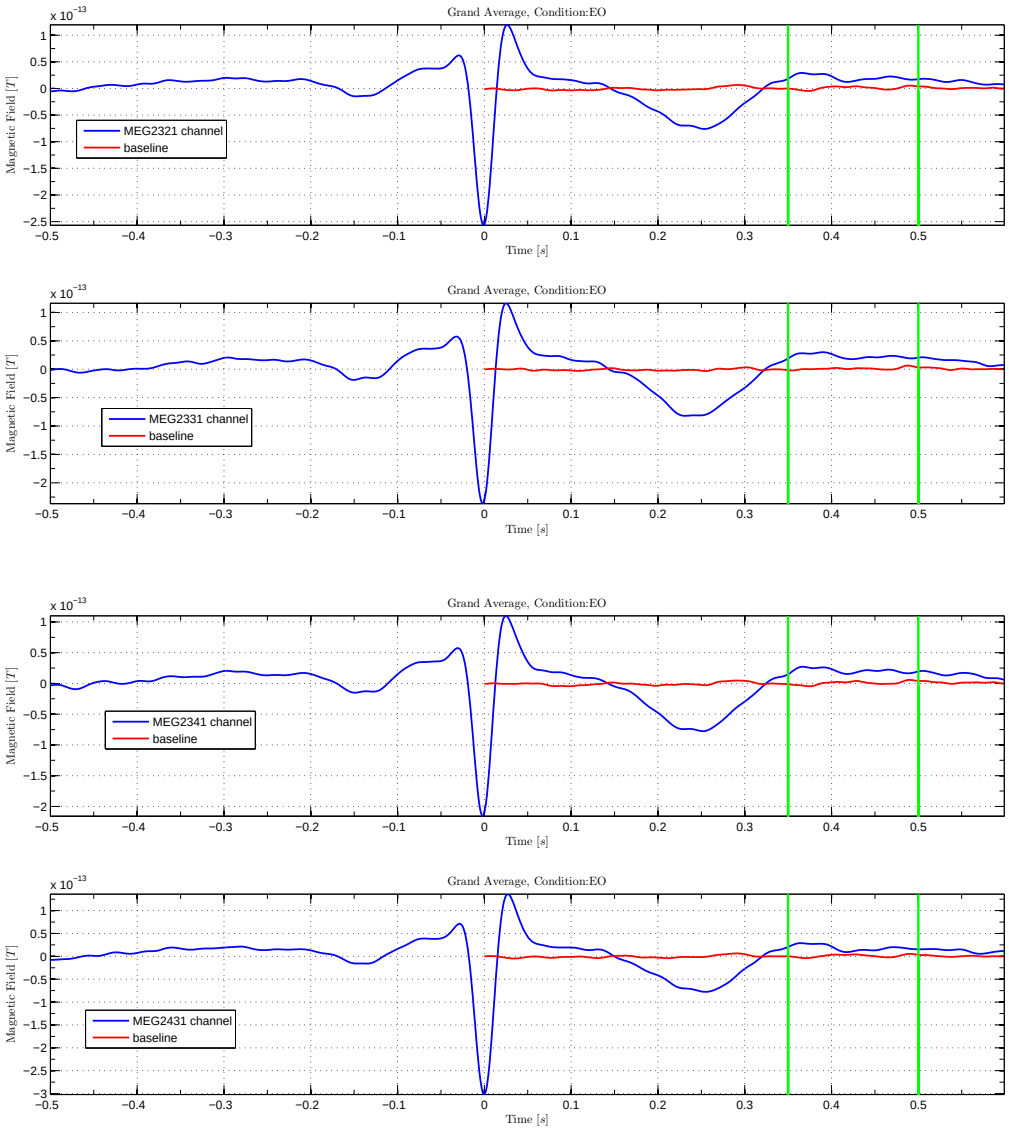

Figure 5.14: Time courses.

5.3 The baseline correction problem

Observing the time courses of the grand average of the ECG, an issue can be easily detected: in the resting time intervals (that is, before the P and after the T waves), $ECG(t)$ is not settled on the chosen baseline. This error is not due to a bias in the recording sensor, otherwise also the baseline would experience the same kind of shift. Therefore, this shift makes inconsistent equation (3.4) and (3.6), invalidating our definition of W_{HER}, due to fact that the results showed that the first equation in (3.5) actually does not hold. Thus, the model for $e(t)$ must be updated as follows:

$$e(t) = e_1(t) + e_2(t), \tag{5.2}$$

where:

- $e_1 \sim \mathcal{N}(0, \sigma^2)$: AWGN $\rightarrow$ $e_1(t) \simeq 0$ because of filtering and averaging.
- $e_2(t)$: sistematic error which causes $ECG(t) \neq \beta_{ECG}\ \forall t \in W_{HER}$.

Therefore, in the multi-subject scenario we have:

$$e(t) \simeq e_2(t) \tag{5.3}$$

Now, if this problem were circumscribed just in the ECG channel, a simple demeaning solution (that is, subtracting the mean value of the pre-stimulus time interval to the whole signal) would be sufficient, since in the ECG there is no HER to be evaluated. However, a similar shift can be observed in the time trend of the magnetometers; calling $\mathscr{P}(e(t))$ such error, we have:

$$q(t) - b(t) = h(t) + \mathscr{P}(e(t)) \quad \forall t \in W_{HER} \tag{5.4}$$

Therefore we need an estimate of $\mathscr{P}(e(t))$ and, due to the similarity of the processes (at least in the locations with good SNR), such estimate can be evaluated from $e(t)$, since in the ECG channel the scenario is easier because there is not the target signal $h(t)$.

Now, given:

$$e_2(t) \sim \mathcal{G}(\mu_{e_2}, \sigma^2_{e_2}), \tag{5.5}$$

where $\mathcal{G}$ is a general random process and $\sigma^2_{e_2} \simeq 0$, as it can be noted by the empirical observations. Thus we have:

$$e_2(t) \simeq \mu_{e_2} = E[e_2(t)] \simeq E[e(t)] = \bar{e} \tag{5.6}$$

To evaluate $\bar{e}$, we focus on W_{HER}, where, from (3.2) and (5.2), it holds:

$$e(t) = ECG(t) - b_{ECG}(t) \ \Rightarrow E[e(t)] = E[ECG(t)] - \beta_{ECG} = \bar{e} \tag{5.7}$$

Now, $\bar{e}$ is related to the unit of measure of $ECG(t)$, so a normalization factor is required. A common normalization factor is the square root of the energy of the signal, so:

$$\bar{e}_N = \frac{\bar{e}}{\sqrt{E_{ECG}}} \tag{5.8}$$

Then, due to the similarity of the processes in the MEG and ECG channel, we can say:

$$\bar{e}_N = \frac{\bar{e}}{\sqrt{E_{ECG}}} \simeq \frac{\mathscr{P}(\bar{e})}{\sqrt{E_q}}, \tag{5.9}$$

where $\mathscr{P}(\bar{e}) = \mathscr{P}(E[e(t)]) \simeq \mathscr{P}(e(t))$, that is the error signal we want to estimate. Therefore:

$$\mathscr{P}(\bar{e}) \simeq \frac{\bar{e}}{\sqrt{E_{ECG}}}\sqrt{E_q} \ \Rightarrow q_{clean}(t) = q(t) - \mathscr{P}(\bar{e}) sgn(q(0)) \tag{5.10}$$

The value $sgn(q(0))$ has been introduced because in some brain locations the heart activity is projected with opposite polarity relative to the ECG.

5.3.1 Remark

The correction explained above makes mandatory an observation about the whole analysis structure: in fact, the estimation of the is carried out using the averaged data, where the statistical assumptions used as the basis for the estimate hold. However, such correction is not appliable on the single trials, because there the noise power is not negligible and the whole mathematical model for the HER does not hold; therefore, there is a lack of resilience in the single subject analysis, since we are not able to get clean signals as input for the statistical test.

5.4 Final results for the MS-analysis

Considering the observation about the $\mathscr{P}(e)$ and its estimate, the final processing protocol is:

1. reading the raw data with band-pass filtering between $1 - 40Hz$;
2. finding the R peaks in the ECG;
3. segmenting the raw data into both R-locked trials and into fixed time-length trials to get the baseline;
4. time-locked robust average of both R-locked and baseline trials;
5. $\mathscr{P}(e)$ estimation and cancellation;
6. cluster based permutation test within subjects.

Therefore, here the results are showed; the visualization steps are the same as before, that is: time window, topography and time courses.

5.4.1 Eyes Closed

The time intervals where a statistically significant difference is observable in each channel are depicted below:

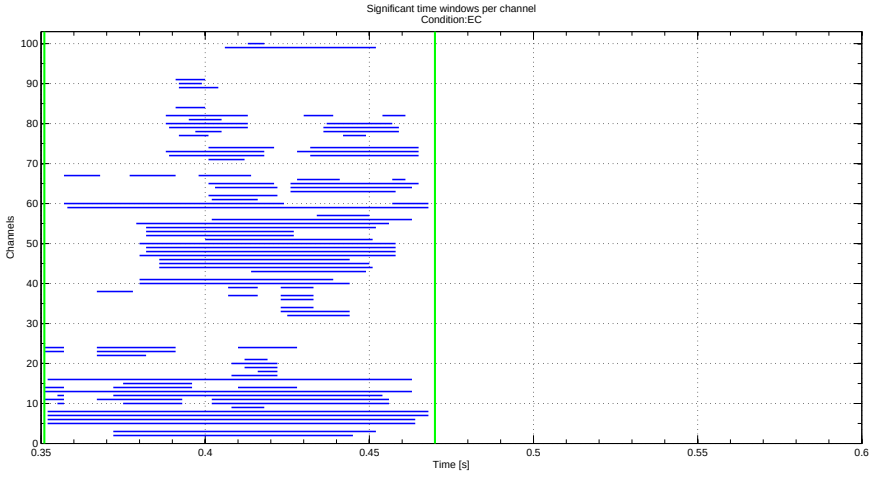

Figure 5.15: Significant time windows for the EC data.

It is immediate to see that the time window shifted on the left, now spanning the $[350\ 470]ms$ interval. The resulting topography at such latency is:

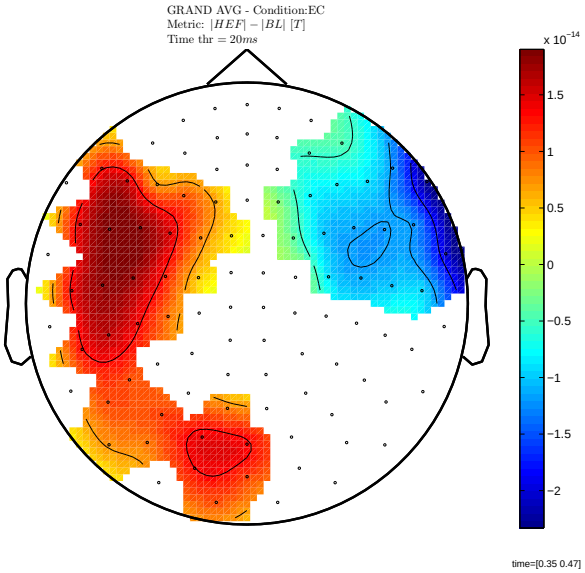

Figure 5.16: Eyes Closed topography.

Thus, a positive difference between the HEF and the baseline is observable in the left pre-frontal,central and occipital areas ($p = 0.001$), while a negative difference is shown in the right pre-frontal zone ($p = 0.002$).

Below few examples of the time course of significant channels are showed.

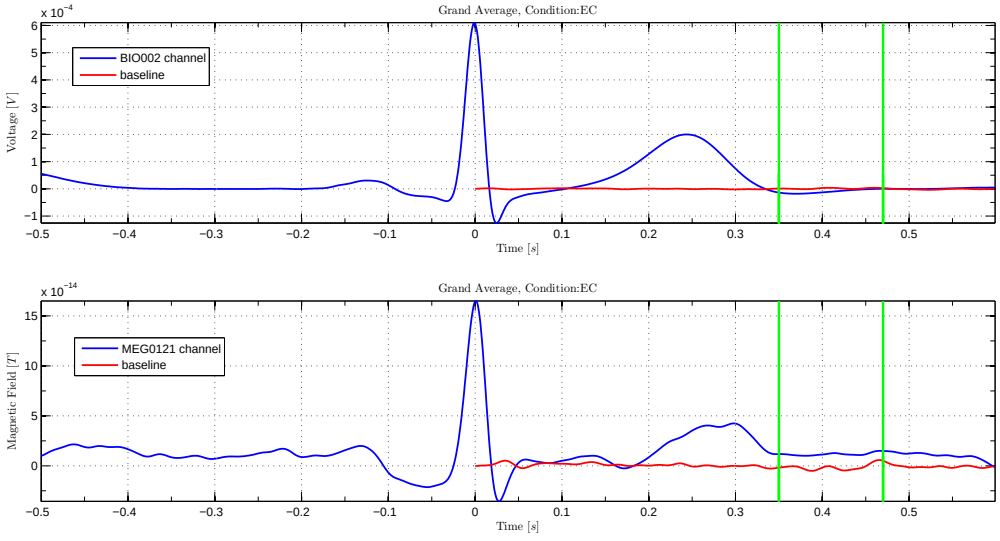

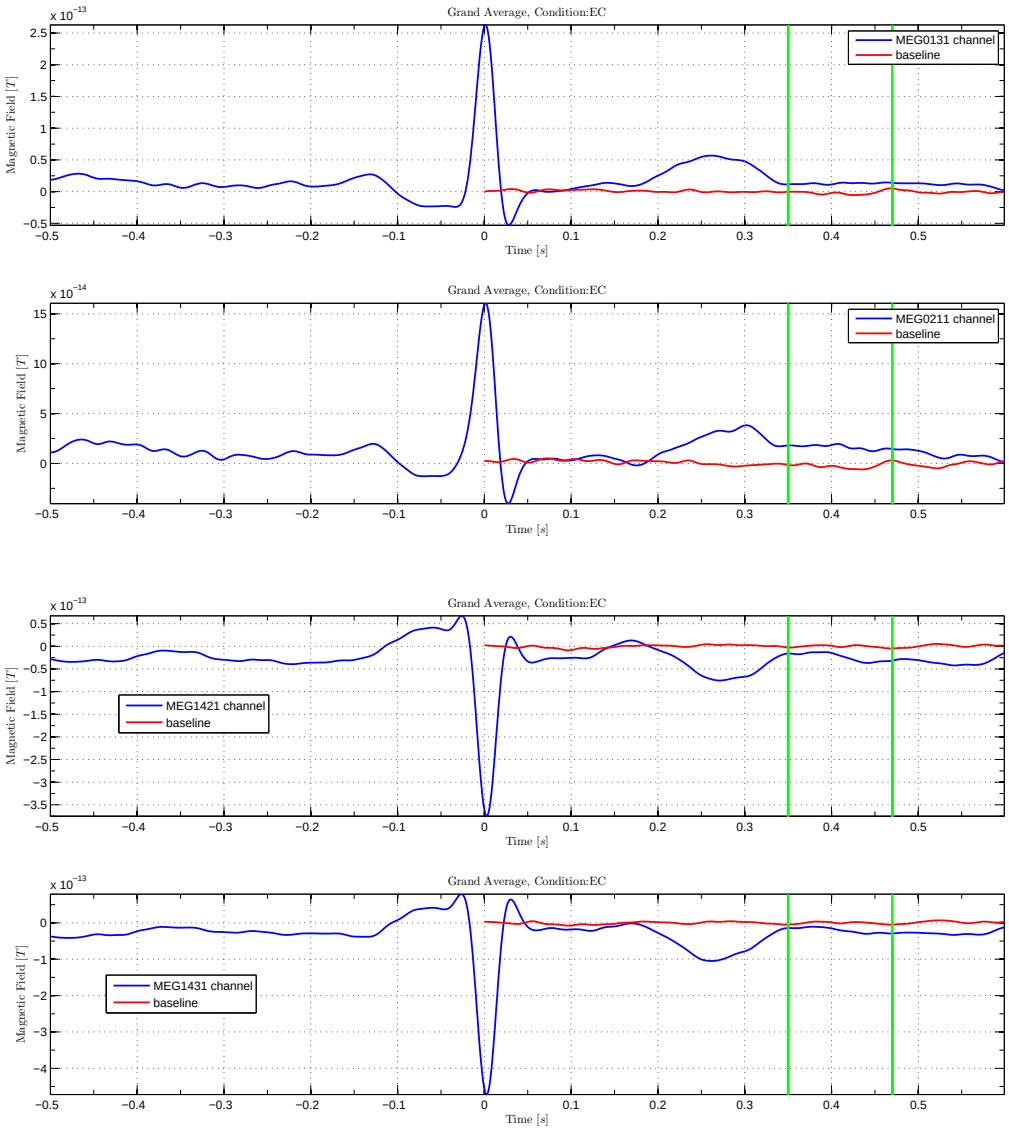
Grand Average, Condition:EC
x 10^-13
Magnetic Field [T]
MEG0131 channel
baseline
Time [s]
Grand Average, Condition:EC
x 10^-14
Magnetic Field [T]
MEG0211 channel
baseline
Time [s]
Grand Average, Condition:EC
x 10^-13
Magnetic Field [T]
MEG1421 channel
baseline
Time [s]
Grand Average, Condition:EC
x 10^-13
Magnetic Field [T]
MEG1431 channel
baseline
Time [s]

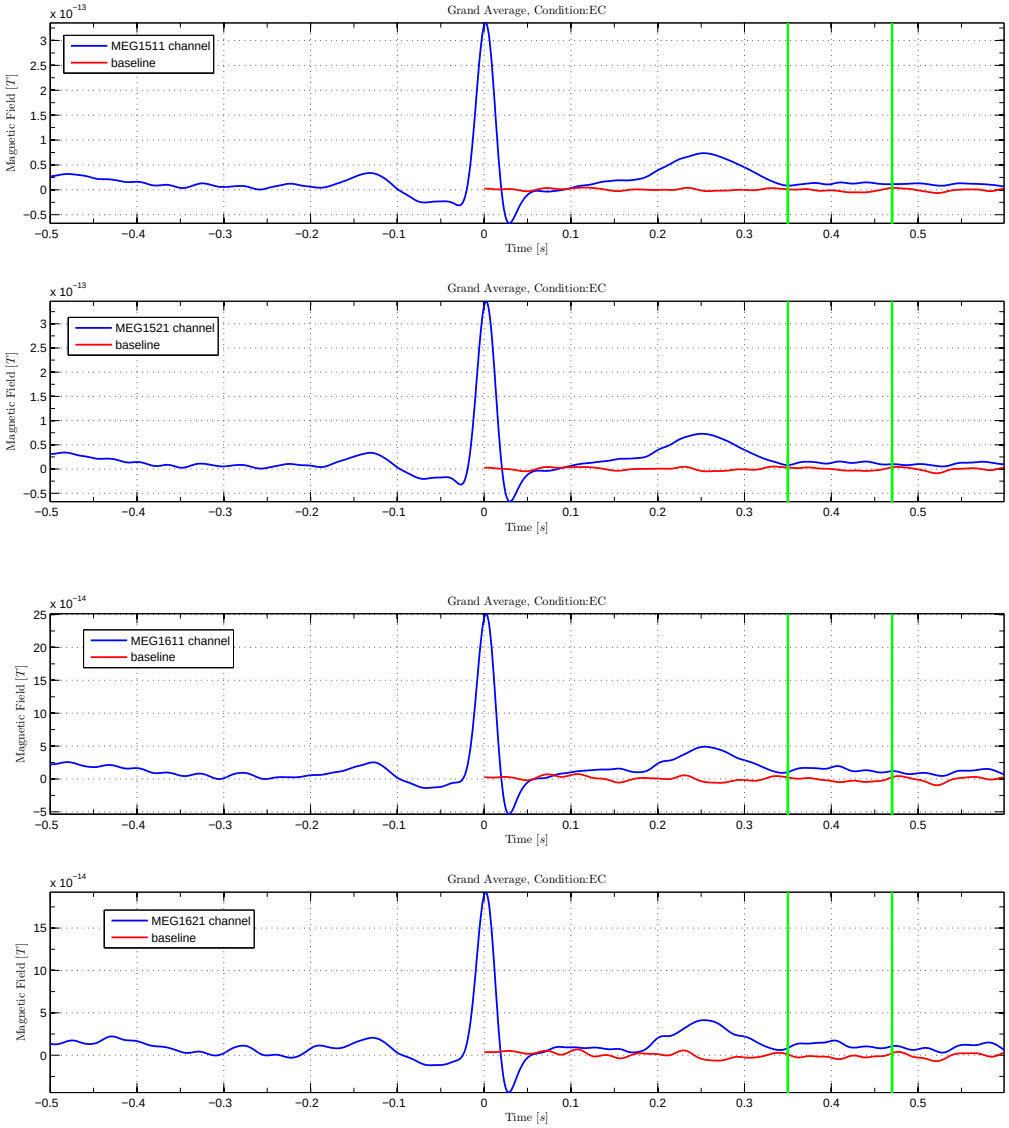

Figure 5.17: Time courses.

It can be noted that now the ECG is well settled on the baseline during the resting intervals, while the MEG channels show a significant difference, positive or negative according to the sign of the R peak.

5.4.2 Eyes Open

Here the results in the Eyes Open case are evaluated.

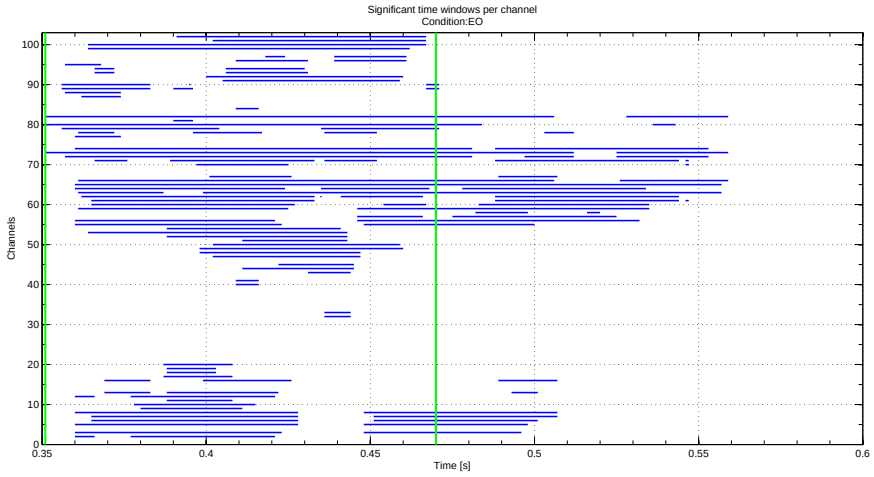

Figure 5.18: Significant time windows for the EO data.

Applying the BL correction, there is much more consistency in the HEF latency: in fact, also in the EO scenario the channels show a significant difference in the [350 470]ms interval. The resulting topography is:

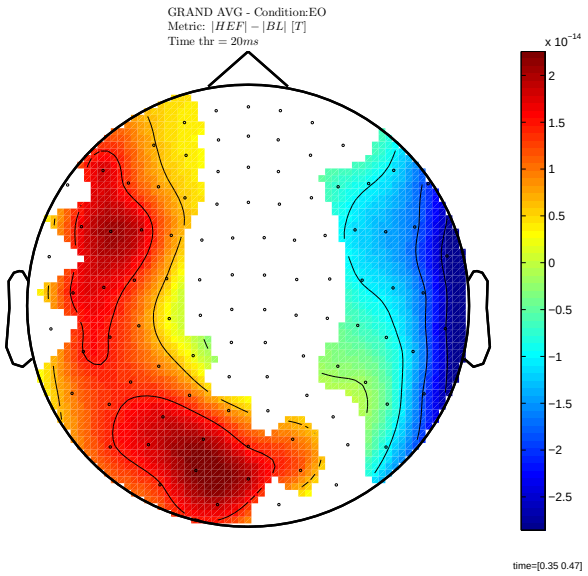

Figure 5.19: Eyes Open topography.

As in the EC case, a positive difference is observable in the left pre-frontal, central and occipital areas ($p = 0.001$), while the negative difference area results a little wider, covering the right pre-frontal, central and a little part of the occipital area ($p = 0.003$). However, the consistency with the EC case is undeniable.

Below few examples of the time course of significant channels are showed.

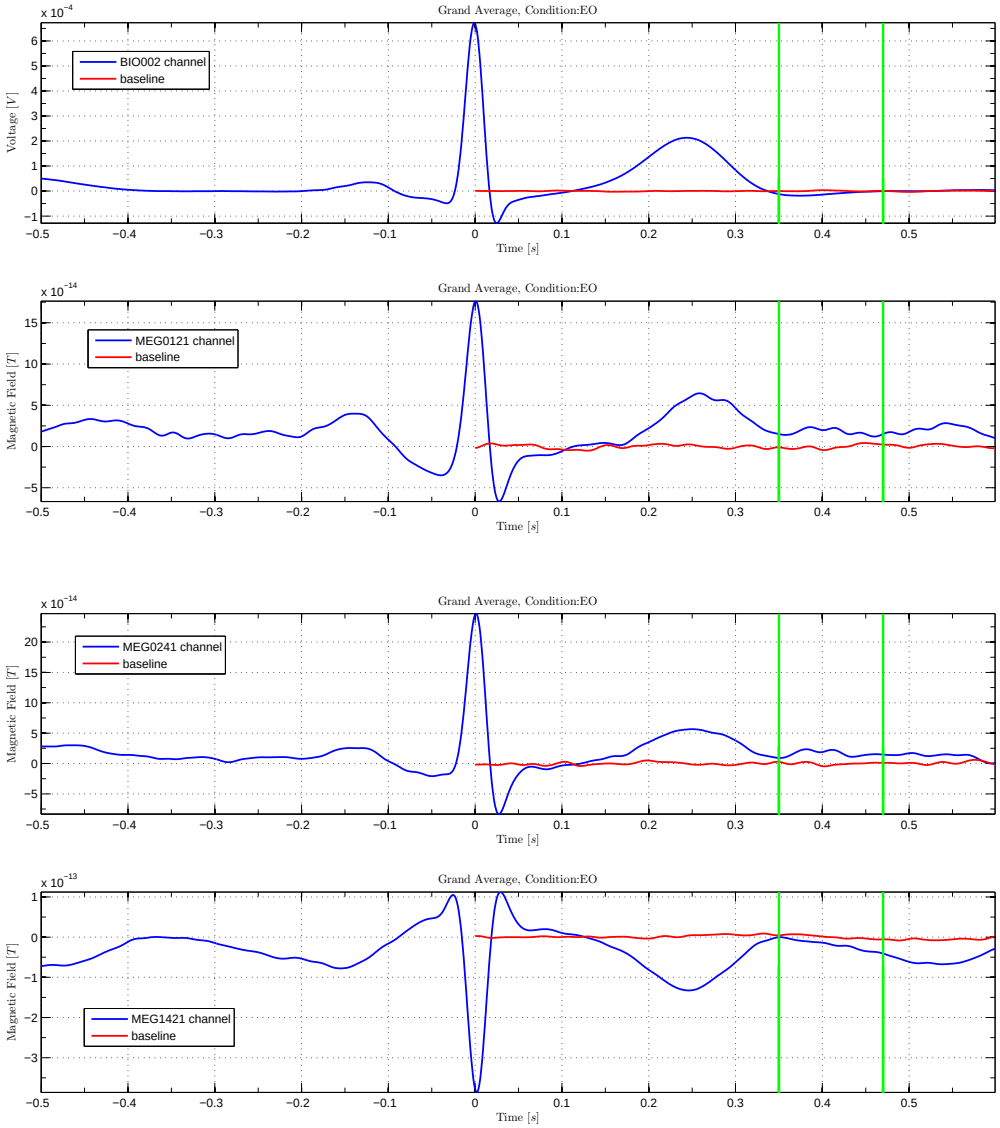
Grand Average, Condition:EO
x 10^-4
BIO002 channel
baseline
Voltage [V]
Time [s]
Grand Average, Condition:EO
x 10^-14
MEG0121 channel
baseline
Magnetic Field [T]
Time [s]
Grand Average, Condition:EO
x 10^-14
MEG0241 channel
baseline
Magnetic Field [T]
Time [s]
Grand Average, Condition:EO
x 10^-13
MEG1421 channel
baseline
Magnetic Field [T]
Time [s]

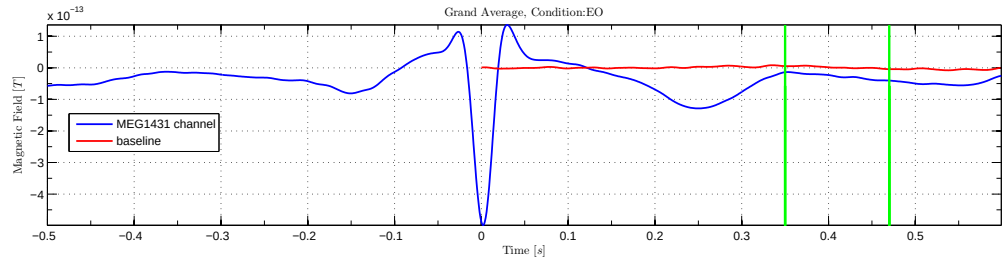
Grand Average, Condition:EO
x 10^-13
Magnetic Field [T]
MEG1431 channel
baseline
Time [s]

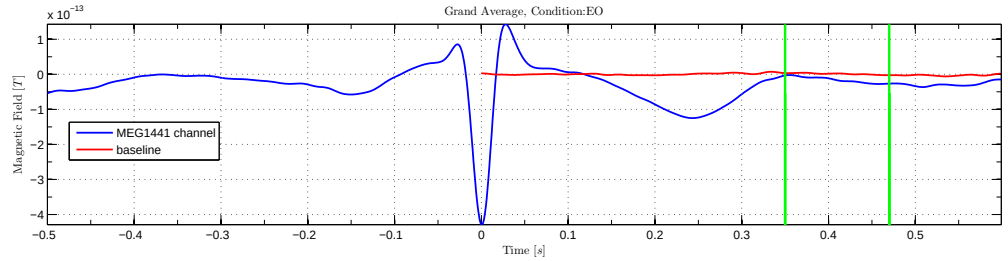
Grand Average, Condition:EO
x 10^-13
Magnetic Field [T]
MEG1441 channel
baseline
Time [s]

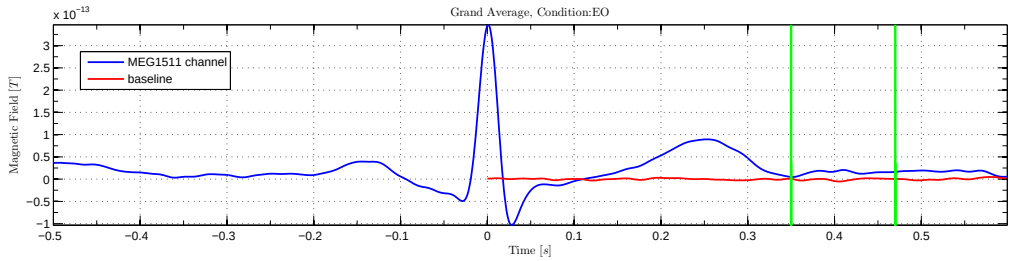
Grand Average, Condition:EO
x 10^-13
Magnetic Field [T]
MEG1511 channel
baseline
Time [s]

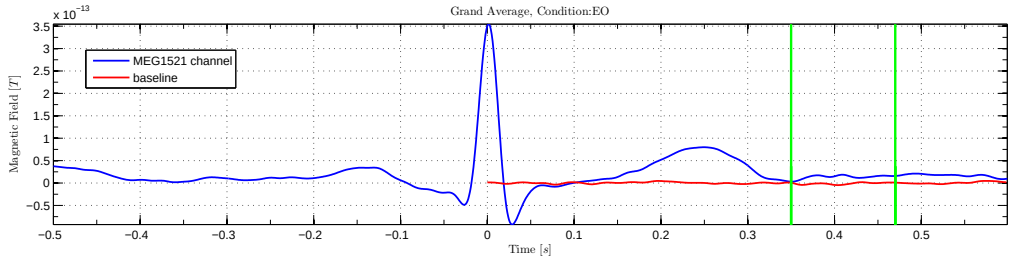
Grand Average, Condition:EO
x 10^-13
Magnetic Field [T]
MEG1521 channel
baseline
Time [s]

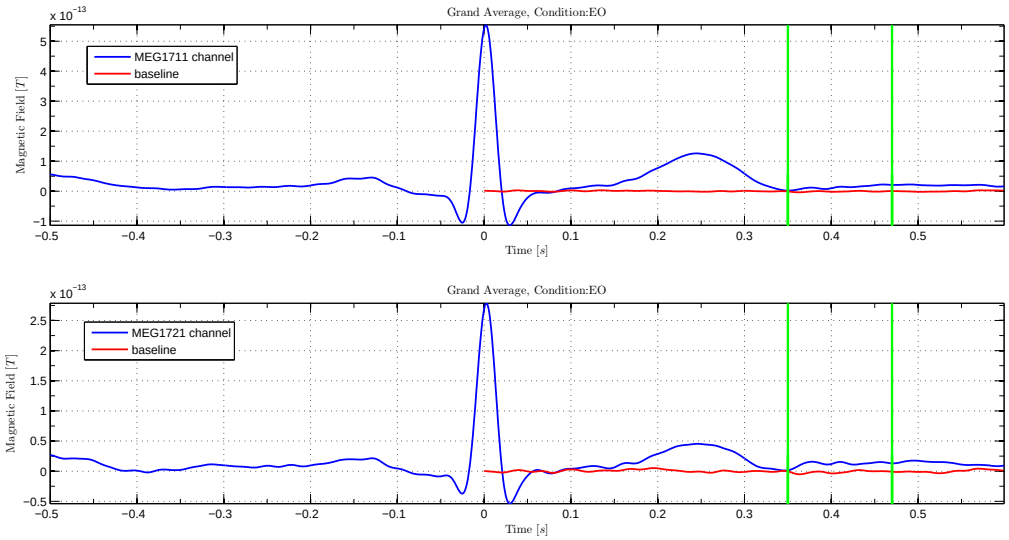

Figure 5.20: Time courses.

5.4.3 Discussion

After the baseline correction, there is consistency in the HEF latency between the Eyes Close and Eyes Open conditions, resulting in the $[350\ 470]ms$ interval after the R peak.
The HEF affects mainly the left pre-frontal, central and occipital areas, but also the right pre-frontal and central areas show significant activation. The amplitude of the magnetic field generated by the HEF spans from $-25fT$ to $20fT$.
Observing the time courses, it can be noted that the HEF trend is not a peak response, but an ongoing almost constant activity. This is consistent with the physiological interpration of the HER, which is thought to be a sort of feedback of the cardiac activity: then the brain registers that a PQRST cycle (that is a heartbeat) has been completed and the ongoing activity monitors the resting period of the heart before the next activation.

5.5 Further developments

Now that reliable results have been achieved, it is interesting to analyse whether there is any feature that might correlate with the HEF; since such response is a cardiac-related phenomenon, a natural question that arises is if the amplitude of the R peak in the ECG somehow influences the trend of the HEF. To answer this question, it is firstly necessary to split the set of subjects into two different and non-overlapping groups: people with an high amplitude of the R peak, that is $ECG(0)$, versus individuals with a small R peak. To do so, a threshold must be established, therefore the amplitudes distribution of the R peaks has to be evaluated through an histogram plot.
Once established a suitable threshold, the two groups will be compared through a

topographic plot depicting the difference between the respective HEF amplitudes, and also through the time courses visualization, to get a more complete picture of the situation.
It has to be observed that the locations taken into account will be just the ones labeled as significant by the statistical test performed between QRS-locked and baseline signals.
Below the results for the Eyes Closed and Eyes Open conditions are reported.

5.5.1 Eyes Closed

The histogram for the R peak amplitudes is the following:

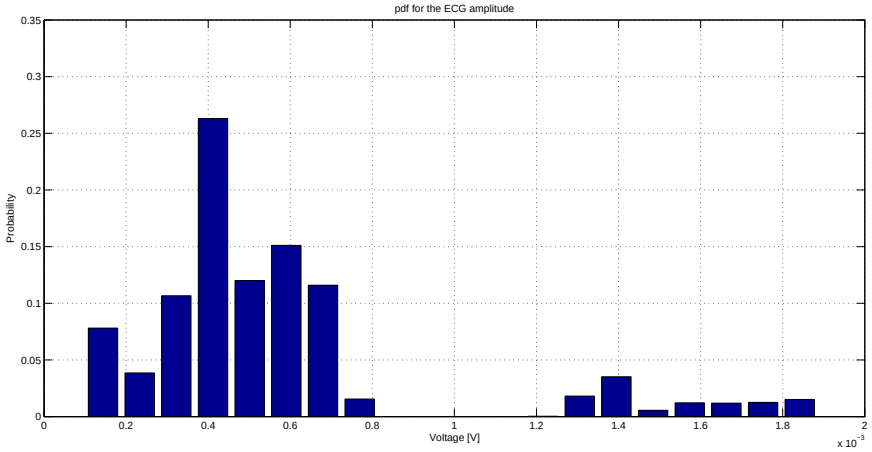

Figure 5.21: R peaks distribution for the EC data.

Therefore, the chosen threshold for the groups partition is $thr = 0.5mV$.
The topography depicting the difference in the HEF amplitude between the two groups is depicted below. Of course the time window considered is the same as in the previous case, since it has been established which is the latency when it is most likely to observe the HEF; thus every further evaluation of the HEF features has to be carried out in such time interval.

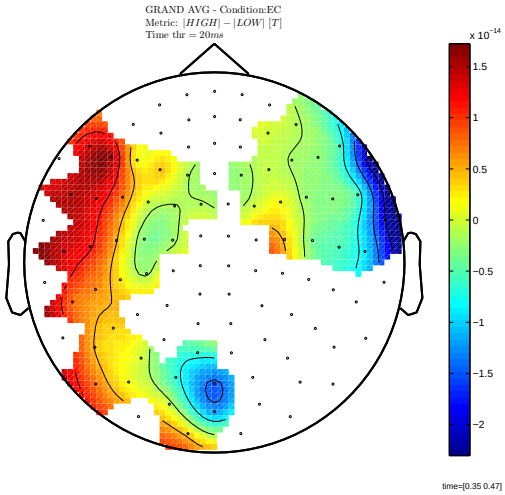

Figure 5.22: Topography of "High R"vs"Low R" HEF amplitude for the EC data.

From the figure, it can be observed that the R peak seems to correlate with the HEF and, in particular, the higher is the R amplitude the higher is the HEF amplitude (in absolute value). Evaluating the time courses, such statement is confirmed:

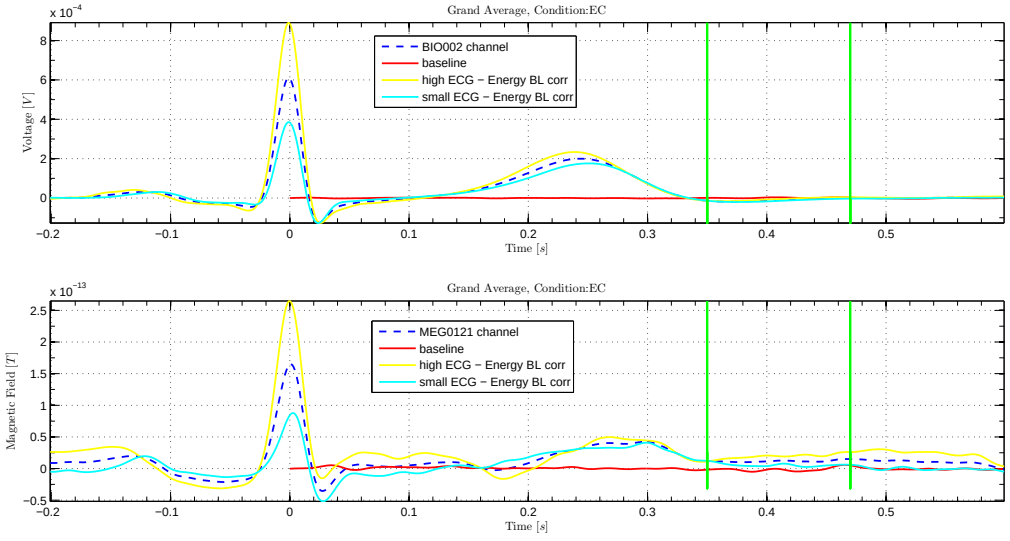

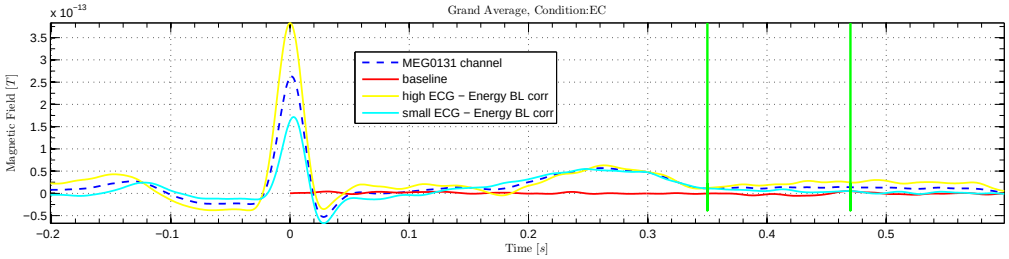
Grand Average, Condition:EC
x 10^-13
Magnetic Field [T]
Time [s]
MEG0131 channel
baseline
high ECG − Energy BL corr
small ECG − Energy BL corr

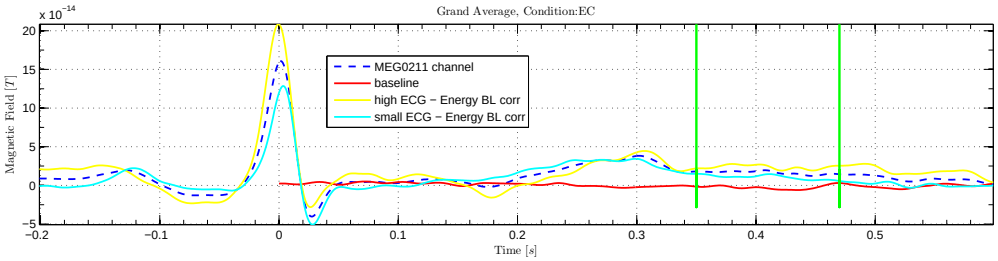
Grand Average, Condition:EC
x 10^-14
Magnetic Field [T]
Time [s]
MEG0211 channel
baseline
high ECG − Energy BL corr
small ECG − Energy BL corr

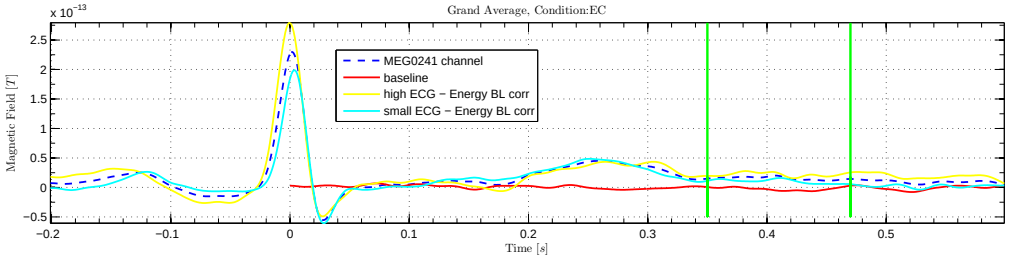
Grand Average, Condition:EC
x 10^-13
Magnetic Field [T]
Time [s]
MEG0241 channel
baseline
high ECG − Energy BL corr
small ECG − Energy BL corr

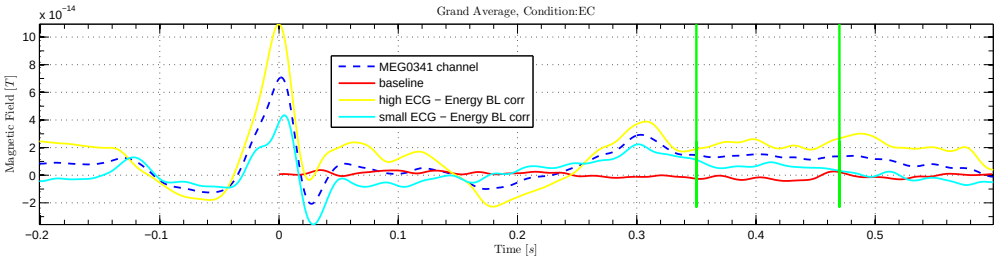
Grand Average, Condition:EC
x 10^-14
Magnetic Field [T]
Time [s]
MEG0341 channel
baseline
high ECG − Energy BL corr
small ECG − Energy BL corr

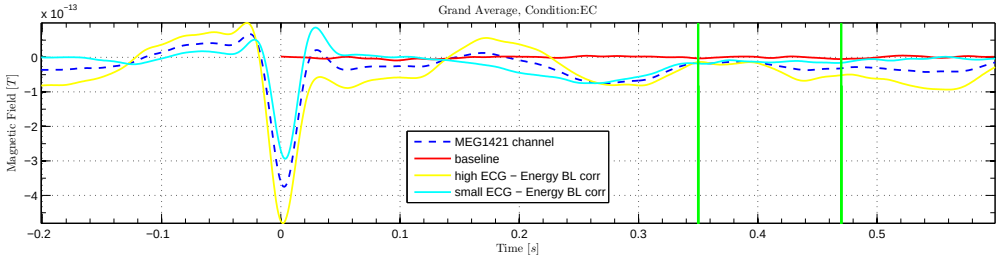
Grand Average, Condition:EC
x 10^-13
Magnetic Field [T]
Time [s]
MEG1421 channel
baseline
high ECG − Energy BL corr
small ECG − Energy BL corr

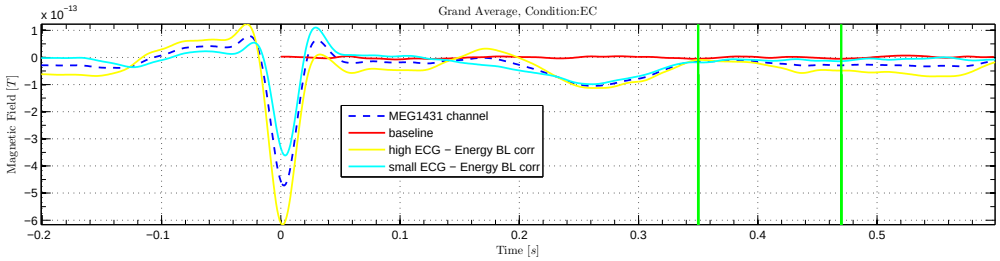
Grand Average, Condition:EC
x 10^-13
Magnetic Field [T]
Time [s]
MEG1431 channel
baseline
high ECG − Energy BL corr
small ECG − Energy BL corr

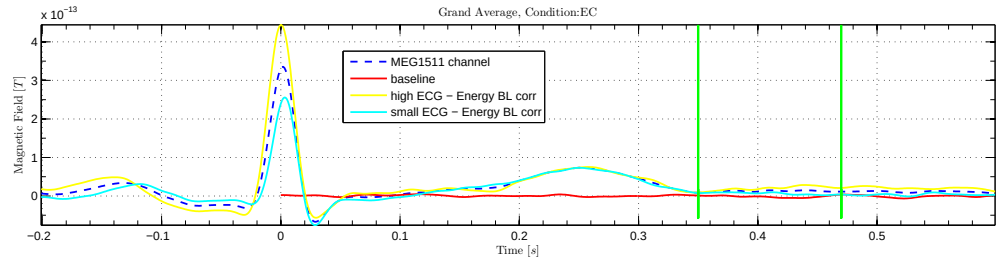
Grand Average, Condition:EC
x 10^-13
Magnetic Field [T]
Time [s]
MEG1511 channel
baseline
high ECG − Energy BL corr
small ECG − Energy BL corr

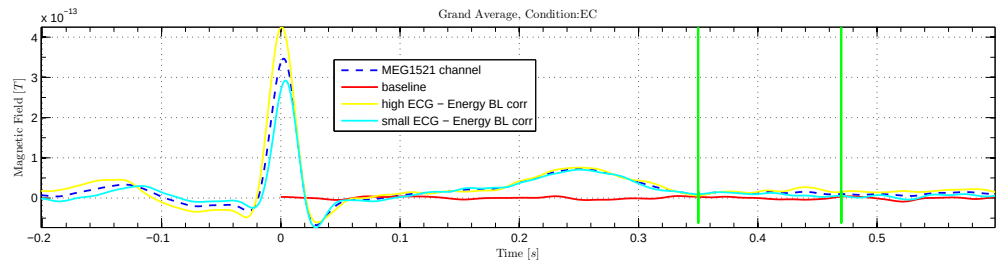
Grand Average, Condition:EC
x 10^-13
Magnetic Field [T]
Time [s]
MEG1521 channel
baseline
high ECG − Energy BL corr
small ECG − Energy BL corr

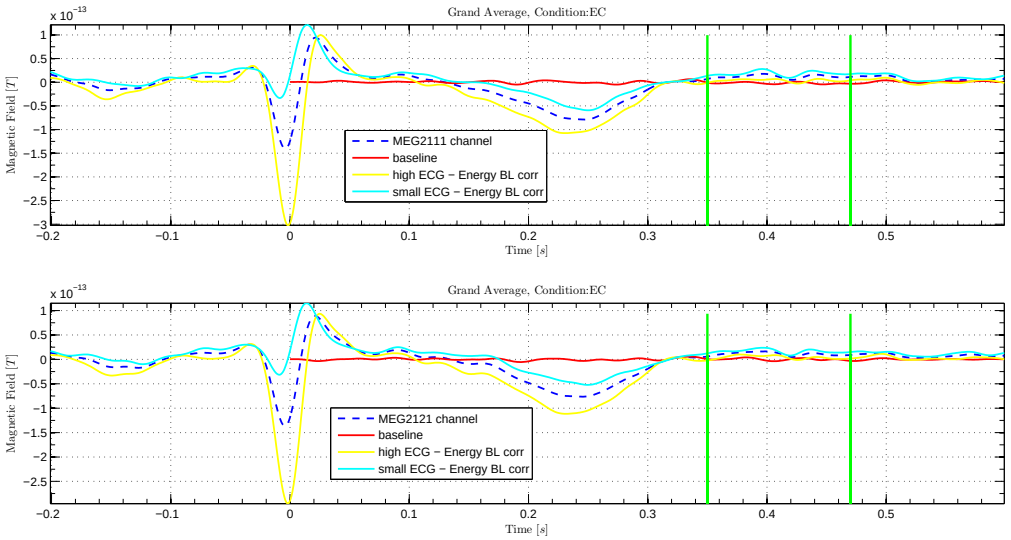

Figure 5.23: Time courses.

5.5.2 Eyes Open

In the Eyes Open case, the histogram for the R peak amplitudes is:

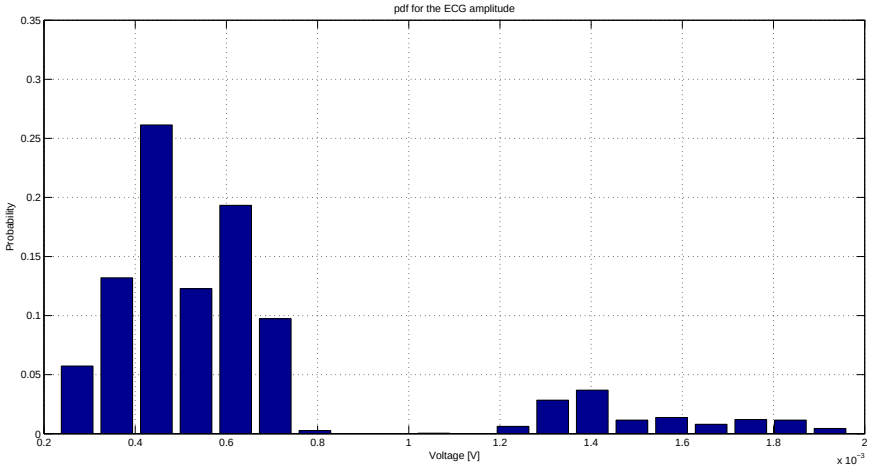

Figure 5.24: R peaks distribution for the EO data.

Thus, also here a suitable threshold for the groups partition is $thr = 0.5mV$. The topography depicting the difference in the HEF amplitude between the two groups is depicted below:

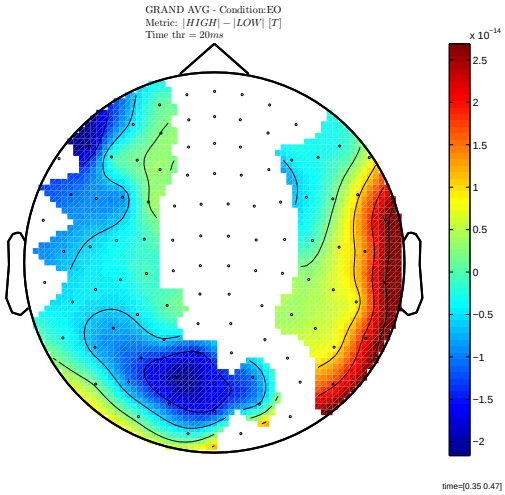

Figure 5.25: Topography of "High R"vs"Low R" HEF amplitude for the EO data.

In this case the result is quite unexpected: in fact the situation looks turned upside down compared with the EC case, since the proportionality is now inverse (the higher the R peak, the smaller the HEF). The evaluation of the time courses is mandatory to get a better insight of the scenario:

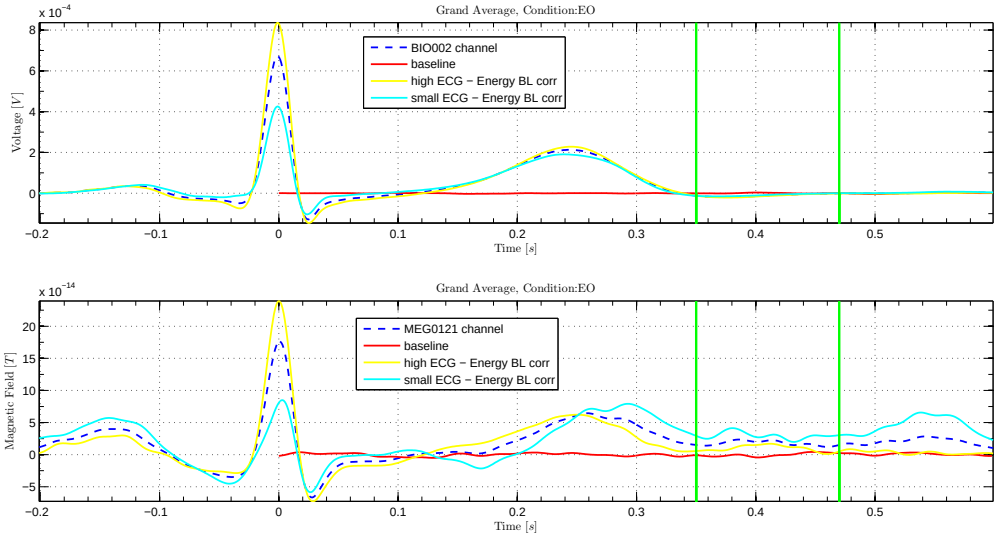

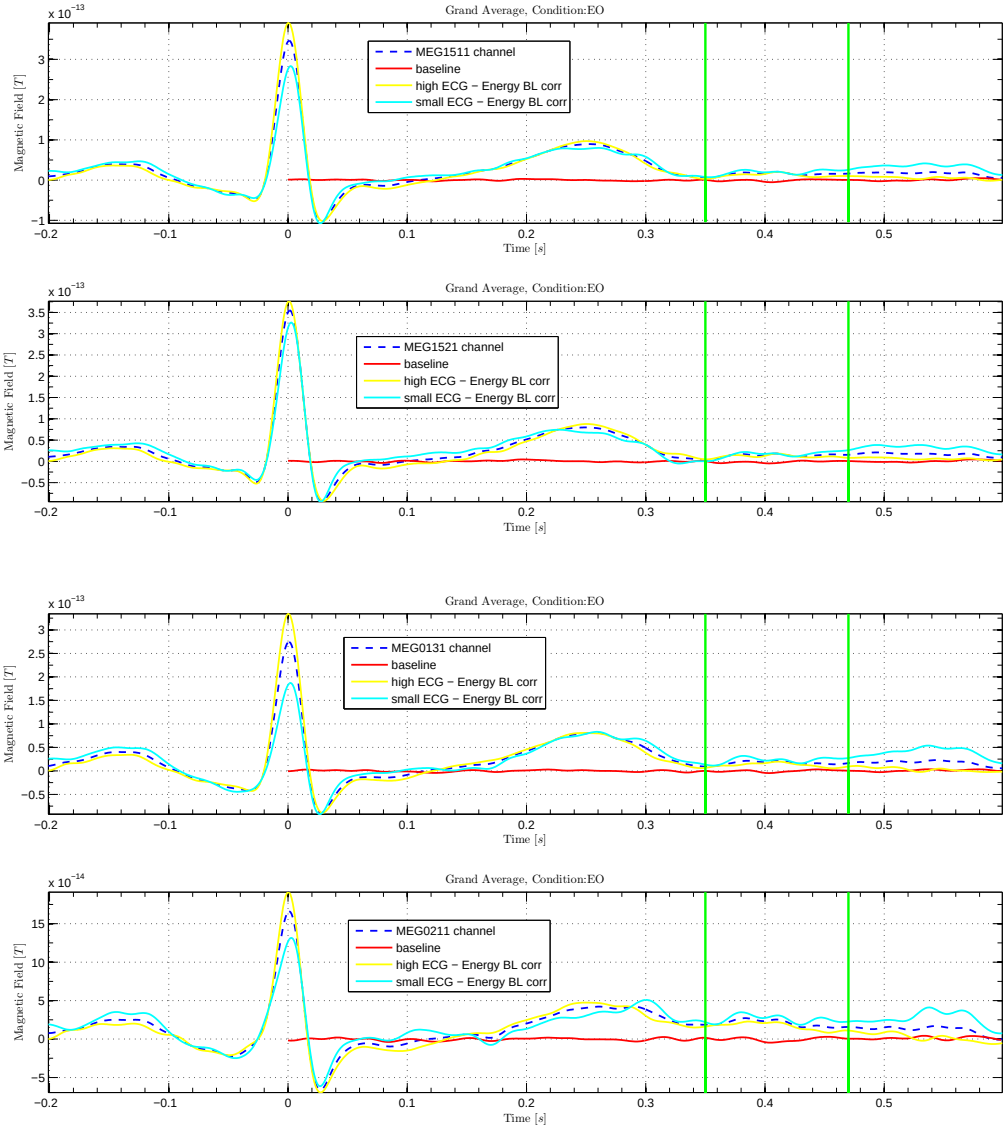
Grand Average, Condition:EO
x 10^-13
MEG1511 channel
baseline
high ECG − Energy BL corr
small ECG − Energy BL corr
Magnetic Field [T]
Time [s]
Grand Average, Condition:EO
x 10^-13
MEG1521 channel
baseline
high ECG − Energy BL corr
small ECG − Energy BL corr
Magnetic Field [T]
Time [s]
Grand Average, Condition:EO
x 10^-13
MEG0131 channel
baseline
high ECG − Energy BL corr
small ECG − Energy BL corr
Magnetic Field [T]
Time [s]
Grand Average, Condition:EO
x 10^-14
MEG0211 channel
baseline
high ECG − Energy BL corr
small ECG − Energy BL corr
Magnetic Field [T]
Time [s]

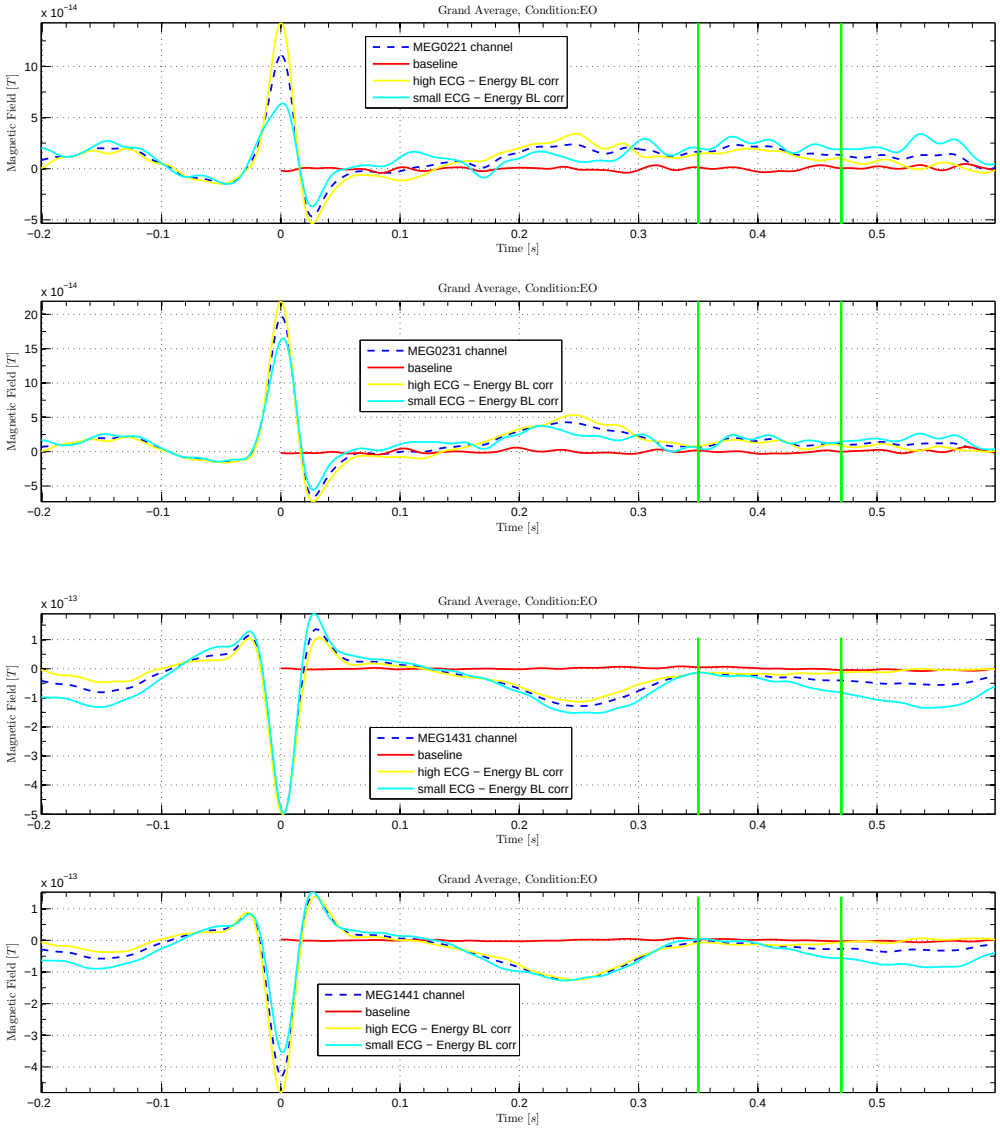
Grand Average, Condition:EO
x 10^-14
MEG0221 channel
baseline
high ECG − Energy BL corr
small ECG − Energy BL corr
Magnetic Field [T]
Time [s]
Grand Average, Condition:EO
x 10^-14
MEG0231 channel
baseline
high ECG − Energy BL corr
small ECG − Energy BL corr
Magnetic Field [T]
Time [s]
Grand Average, Condition:EO
x 10^-13
MEG1431 channel
baseline
high ECG − Energy BL corr
small ECG − Energy BL corr
Magnetic Field [T]
Time [s]
Grand Average, Condition:EO
x 10^-13
MEG1441 channel
baseline
high ECG − Energy BL corr
small ECG − Energy BL corr
Magnetic Field [T]
Time [s]

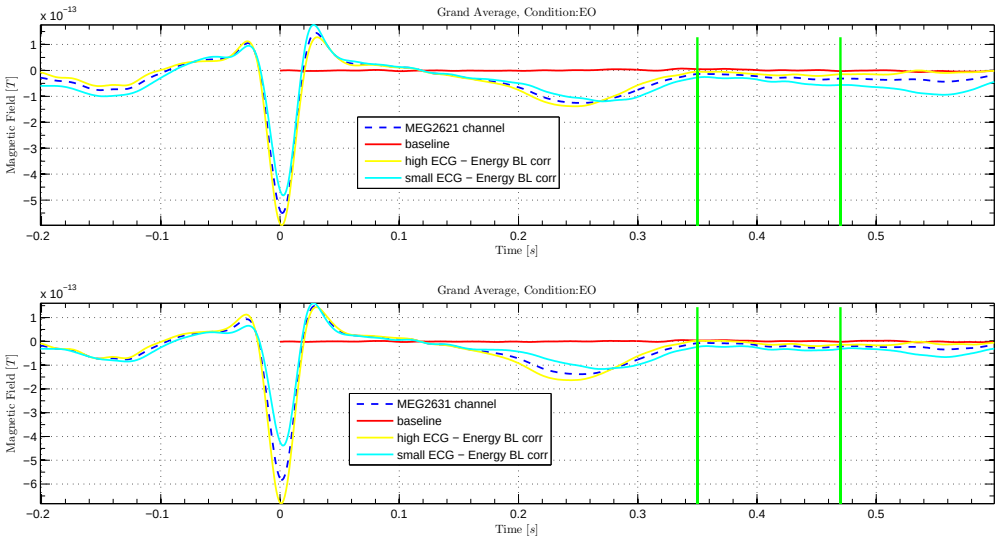

Figure 5.26: Time courses.

The time trends confirm that the subjects with a lower R peak show a higher amplitude, in absolute value, of the HEF.

5.5.3 Discussion

The study of the correlation between the amplitude of the R peak and the one of the HEF led to quite contrasting results: in the Eyes Closed case, the relationship between the two quantities is a direct proportionality, while in the Eyes Open scenario the proportionality is inverse. Nevertheless, the existence of a correlation between the R peak and the HEF is very likely. The difference in the obtained results might just be due to a lower SNR in the Eyes Open case because of the smaller number of subjects in such dataset: in particular, the group of "low R peak" has just 6 subjects, which might be to small to get a reliable average.

Chapter 6

The Source Analysis

The MEG signals measured on the scalp do not directly reflect the location of the activated neurons, thence a technique to reconstruct the location and the time course (or spectral content) of a source in the brain is required. To this aim, various source localization methods are available, such as dipole fitting, distributed models, scanning methods. However, all of them share the same underlying structure: estimating, given a suitable model, the current sources in the brain fom the MEG data.

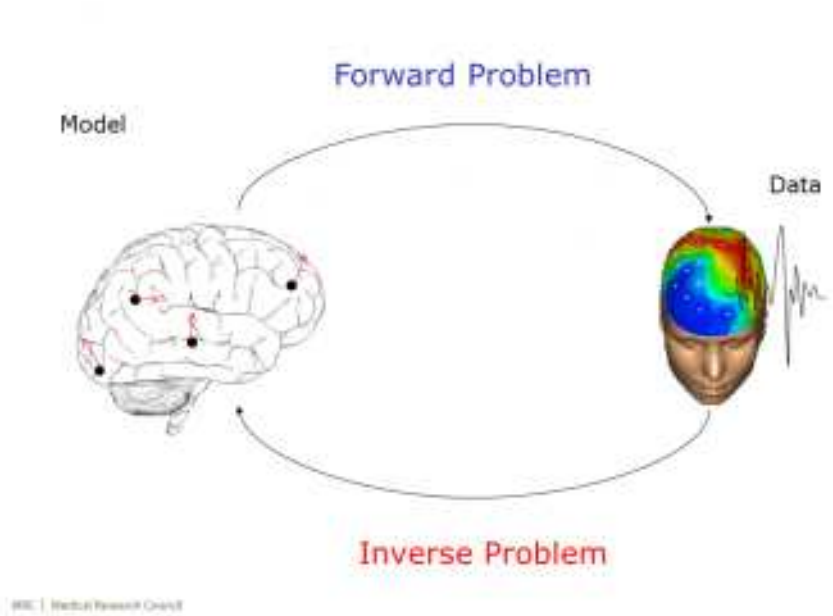

Figure 6.1: General structure of the source analysis.

The level of the activity at a source location is estimated from:

- the MEG activity measured around the scalp;
- the spatial arrangement of the sensors (channel positions);

- the geometrical and electrical/magnetic properties of the head (head model);
- the location of the sources (source model);

Using this information, source estimation comprises two major steps:

1. Estimation of the potential or field distribution for a known source and for a known model of the head is referred to as forward modeling.
2. Estimation of the unknown sources corresponding to the measured EEG or MEG is referred to as inverse modeling.

The forward solution can be computed when the head model, the channel positions and the source is given. A prerequisite of forward modeling is that the geometrical description of all elements (channel positions, head model and source model) is registered in the same coordination system with the same units. There are different "conventions" how to define a coordinate system, but the precise coordinate system is not relevant, as long as all data is expressed in it consistently (i.e. in the same coordinate system). The MEG sensors by default are defined relative to anatomical landmarks of the head (the fiducial coils), therefore when the anatomical images are also aligned to these landmarks, the MEG sensors do not need to be re-aligned.
The inverse problem is the actual source localization problem and, as commented before, there are various solutions available. The method adopted in this work is a scanning technique, in particulare the Linearly Constrained Minimum Variance (LCMV) Beamformer.

6.1 The forward model

The first requirement for the source reconstruction procedure is that we need a forward model. The forward model allows us to calculate the distribution of the magnetic field on the MEG sensors given a hypothetical current distribution. The forward models for MEG are typically constructed for each subject individually, taking the position and especially the size of the head into account. The size of the head determines the distance between brain and MEG sensors, the larger the distance, the weaker the cortical sources will be observed by the MEG sensors. Thus, at the sensor level, the recorded MEG signal is actually the result of a superimposition of the source activity, due to the following reasons:

- there is a varying "visibility" of each source to each channel (sensor);
- the time course of each source contributes to each channel;
- the contribution of each source depends on its "visibility".

Thus, being $\mathbf{x(t)}$ $(M \times 1)$ the MEG signal at the time t, we have (omitting the time index to ease the notation):

$$\mathbf{x} = \mathbf{H(q)s(q)} \tag{6.1}$$

where:

- $\mathbf{q}$ (3×1) is the source location, that is the vector with the 3-D coordinates representing a certain area in the brain volume;

- **H** is the *leadfield*, that is how each source is visible at the channel level. In a more formal physical sense, **H** represents the material and geometrical properties of the medium in which the sources are submerged;

- $\mathbf{s}(\mathbf{q})$ is the vector with the x, y, z components of the dipole moment at the time t, that is the activity of the source in the location $\mathbf{q}$ at the time t.

Now, supposing L active dipoles at locations $\mathbf{q}_i,\ i = 1, \ldots, L$, the actual MEG signal recorded by the M sensors at the time t is:

$$\mathbf{x} = \sum_{i=1}^{L} \mathbf{H}(\mathbf{q}_i)\mathbf{s}(\mathbf{q}_i) + \mathbf{n}, \tag{6.2}$$

where $\mathbf{n}$ is the measurement noise. To compute the leadfield we need: the position of the MEG sensor related to the brain, the volume conduction model of the head, and the position of potential sources. The first is easily provided by the gradiometers definition in the MEG data; the computation of the other two is instead less trivial and is detailed below.

6.1.1 The volume conduction model

The volume conduction model is necessary to get a description of the electrical properties of the tissues and their geometry, being then a physical and geometrical approximation of the head. However, it just describes how the currents flow through the tissue, not where they originate from.
In general it consists of a description of the geometry of the head, a description of the conductivity of the tissue, and mathematical parameters that are derived from these. Whether and how the mathematical parameters are described depends on the computational solution to the forward problem either by numerical approximations, such as the boundary element and finite element method (BEM and FEM), or by exact analytical solutions (e.g. for spherical models). The more accurate the description of the geometry of the head or the source, the better the quality of the forward model. There are many types of head models which, to various degrees, take the individual anatomy into account.
In this work we will use a semi-realistic head model developed by [19] that assumes a realistic information about the interface between the brain and the skull and it is based on a correction of the leadfield for a spherical volume conductor by a superposition of basis functions, gradients of harmonic functions constructed from spherical harmonics.
The first step in constructing the head model is to find the brain surface from the subjects MRI. Each of the voxels of the anatomical MRI is assigned to a tissue class: this procedure is termed segmentation since in this step, the voxels of the anatomical MRI are segmented (i.e. separated) into different tissue types. By default, the gray matter, white matter and the cerebro-spinal fluid (csf) compartments are differentiated. Based on these compartments a so called brainmask is created, which is a binary mask of the content inside the skull. All voxels that are inside the skull (i.e. the complete brain) are represented by 1, all other voxels by 0.
Once the brain mask is segmented out of the anatomical MRI, a surface description

of the brain is constructed using the Nolte's model and the volume conduction model is then created.

6.1.2 The source model

For distributed source models and for scanning approaches (such as beamforming), the source model is discretizing the brain volume into a volumetric or surface grid.
When the forward solution is computed, the leadfield matrix (that is, channels X source points matrix) is calculated for each grid point taking into account the head model and the channel positions.
When conducting a multiple-subject study, it is essential that averaging over subjects does not violate any statistical assumption. One of these assumptions is that subject's sources are represented in a common space, i.e. an averaged grid point represents the estimate of the same brain region across subjects. One way to get subjects in a common space is by spatially deforming and interpolating the source reconstruction after beamforming. However, there exist an alternative way that does not require interpolation, that is using a regular grid in MNI template space and spatially deform this grid to each of the individual subjects. The beamformer estimation is done on the direct grid mapped to MNI space, so that the results can be compared over subjects.

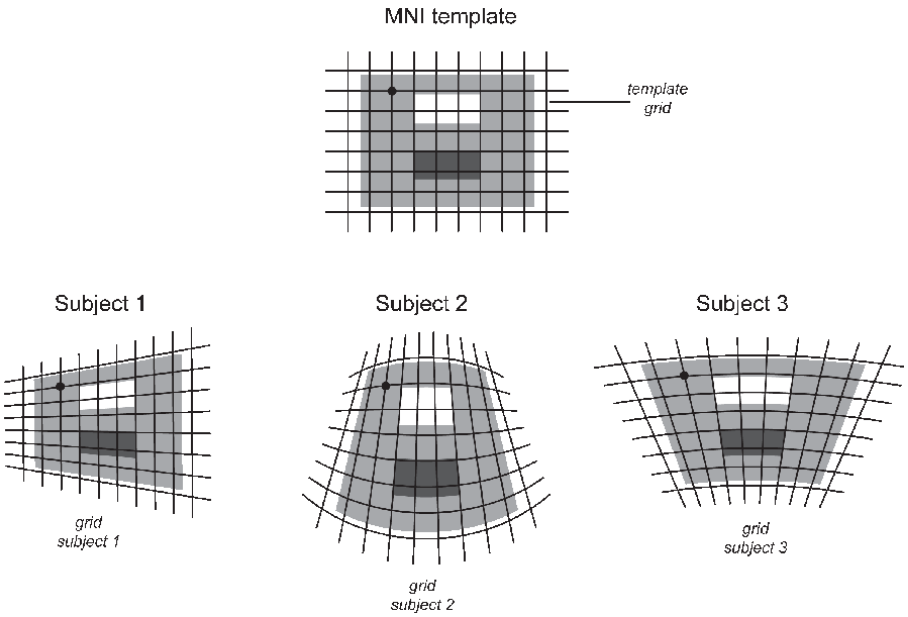

Figure 6.2: The warping on a common MNI grid.

6.2 The inverse problem

The experimental and clinical problem is the inverse problem: the field is sampled at different sensor locations and the underlying activity pattern must be determined.

A given set of measurements cannot generate a unique solution for the activities inside the head. To obtain a single inverse solution for a given recording, additional constraints are introduced. A problem common to all methods is determining the number of active areas that contribute to the signal studied. Here we adopt a localization method based on the principles of spatial filtering, in particular the LCMV beamformer adopted in [20]. Spatial filters are designed that pass brain electrical activity from a specified location while attenuating activity originating at other locations. The power at the output of a spatial filter is an estimate of the neural power originating within the spatial passband of the filter. A map of neural power as a function of location is obtained by designing multiple spatial filters, each with a different passband, and depicting output power as a function of passband location.

The LCMV approach is based on the concept of spatial filtering. Spatial filtering refers to discrimination of signals on the basis of their spatial location. This concept completely parallels the more familiar temporal filtering, where one discriminates between signals based on their temporal frequency content. Hence, a "narrowband" spatial filter passes signals originating from a small "passband" volume while attenuating those originating from other locations. Temporal filtering involves operating on time samples of a signal; spatial filtering involves processing spatial samples of a signal. In our scenario, the spatial samples are elements of the data vector $\mathbf{x}$ and the spatial filter is implemented as a weighted combination of these samples. The goal is to get a bank of spatial filters where each filter passes signals originating from a specified location within the brain while attenuating signals from other locations. A display of the variance or power at the output of each filter as a function of the filter's spatial "passband" location provides an estimate of the distribution of activity within the brain.

6.2.1 The mathematical model

The electrical activity of an individual neuron is a random process influenced by external inputs to the neuron, therefore $\mathbf{s}(\mathbf{q}_i)$ is a random quantity, describable through the mean, $\bar{\mathbf{s}}(\mathbf{q}_i) = E[\mathbf{s}(\mathbf{q}_i)]$, and the covariance matrix, $\mathbf{C}(\mathbf{q}_i) = E[(\mathbf{s}(\mathbf{q}_i) - \bar{\mathbf{s}}(\mathbf{q}_i))(\mathbf{s}(\mathbf{q}_i) - \bar{\mathbf{s}}(\mathbf{q}_i))^T]$.
Assuming a noise such as $E[\mathbf{n}] = 0$ and with covariance matrix $\mathbf{Q}$, and also that the moments associated with different dipoles are uncorrelated, we have:

$$\bar{\mathbf{s}}(\mathbf{x}) = E[\mathbf{s}(\mathbf{x})] = \sum_{i=1}^{L} \mathbf{H}(\mathbf{q}_i)\bar{\mathbf{s}}(\mathbf{q}_i) \tag{6.3}$$

$$\mathbf{C}(\mathbf{x}) = \sum_{i=1}^{L} \mathbf{H}(\mathbf{q}_i)\mathbf{C}(\mathbf{q}_i)\mathbf{H}^T(\mathbf{q}_i) + \mathbf{Q} \tag{6.4}$$

Now, the variance associated with a particular source is a measure of the strength of the source and it is defined as the sum of variance of each component of the dipole moment, that is:

$$var(\mathbf{q}) = tr\{\mathbf{C}(\mathbf{q})\} \tag{6.5}$$

Then, since the signal at each location in the brain consists of the three component dipole moment, we need three spatial filters for each location, one for each component of the dipole moment. Thus, we can define the spatial filter for the narrowband volume element Q_0 centered on location $\mathbf{q}_0$ as:

$$\mathbf{y} = \mathbf{W}^T(\mathbf{q}_0)\mathbf{x}. \tag{6.6}$$

The ideal requirements for the filter are:

$$\mathbf{W}^T(\mathbf{q}_0)\mathbf{H}(\mathbf{q}) = \begin{cases} \mathbf{I} & \mathbf{q} = \mathbf{q}_0 \quad (6.7) \\ \mathbf{0} & \mathbf{q} \neq \mathbf{q}_0,\ \mathbf{q} \in \Omega \quad (6.8) \end{cases}$$

The constraint 6.7 can be fulfilled, but 6.8 is generally unfeasible. Thus, it is required a filter $\mathbf{W}(\mathbf{q}_0)$ that minimizes the variance at the filter output, while satisfying the linear response constraint 6.7. Therefore the problem is:

$$\min_{\mathbf{W}(\mathbf{q}_0)} \quad tr\{\mathbf{C}(\mathbf{y})\} \quad \text{s.t. } \mathbf{W}^T(\mathbf{q}_0)\mathbf{H}(\mathbf{q_0}) = \mathbf{I}, \tag{6.9}$$

that is:

$$\min_{\mathbf{W}(\mathbf{q}_0)} \quad tr\{\mathbf{W}^T(\mathbf{q}_0)\mathbf{C}(\mathbf{x})\mathbf{W}(\mathbf{q}_0)\} \quad \text{s.t. } \mathbf{W}^T(\mathbf{q}_0)\mathbf{H}(\mathbf{q_0}) = \mathbf{I}, \tag{6.10}$$

whose solution is finally:

$$\mathbf{W}(\mathbf{q}_0) = \left[\mathbf{H}^T(\mathbf{q}_0)\mathbf{C}(\mathbf{x})^{-1}\mathbf{H}(\mathbf{q}_0)\right]^{-1}\mathbf{H}^T(\mathbf{q}_0)\mathbf{C}^{-1}(\mathbf{x}) \tag{6.11}$$

Now, from 6.1 and the assumption $E[\mathbf{n}] = 0$, the equation 6.6 is actually the estimate of the source activity, that is:

$$\hat{\mathbf{s}}(\mathbf{q}) = \mathbf{y} = \mathbf{W}^T(\mathbf{q})\mathbf{x}. \tag{6.12}$$

6.3 Results

The computation of $\hat{\mathbf{s}}(\mathbf{q})$ was done for every subject, both for the QRS-locked and baseline signals (using the Eyes Closed data set); then, the results were statistically compared using the cluster based permutation t test, in order to evaluate where there was a significant difference between the two conditions. The following pictures show the areas significantly activated ($p = 0.0012$).

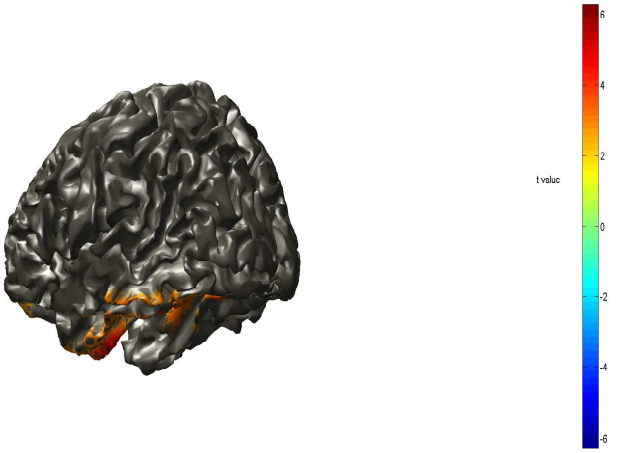

Figure 6.3: Neuronal sources on a whole brain render.

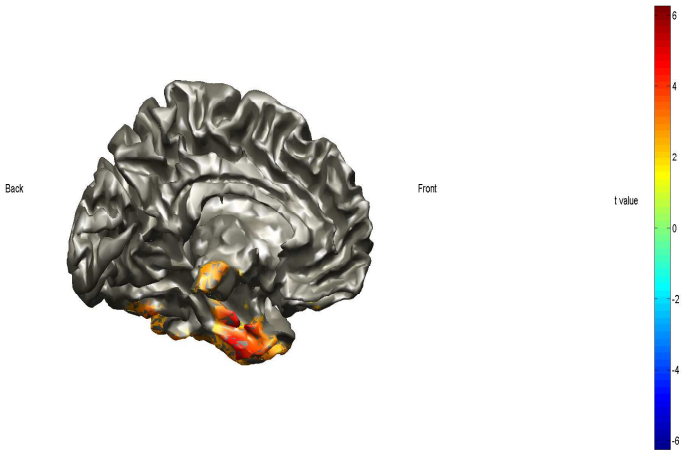

Figure 6.4: Midsagittal section of the left hemisphere.

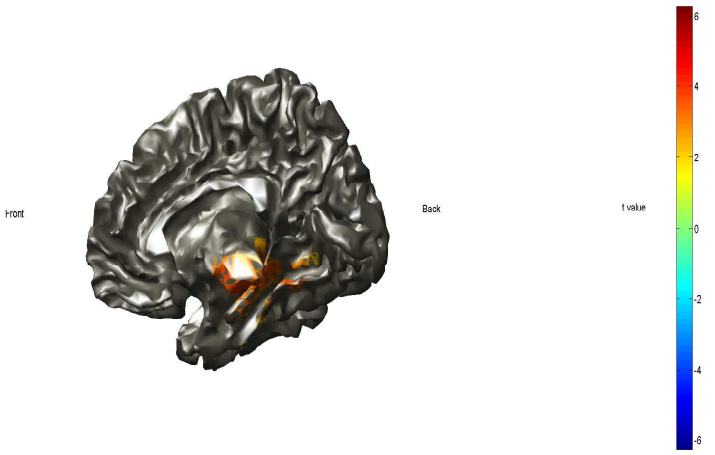

Figure 6.5: Midsagittal section of the right hemisphere.

The locations provided by the Automated Anatomical Labeling (AAL) [21] of the significant areas are summarised in the following table:

Region	x	y	z	t value	Trend
Cerebral peduncle	-53	-54	-50	4.78	Decreasing
Cerebellum	9	-60	-10	3.4	Decreasing
Inferior temporal gyrus	-33	-10	-37	4.5	Decreasing
Thalamus	15	-28	2	3.42	Decreasing
Parahippocampal gyrus	-24	-10	-30	4.94	Decreasing

6.3.1 Discussion

First of all, the areas showing a significant activation are consistent with the ones found in the source-space analysis, as it can be seen from the following picture and recalling that the magnetometers are sensistive to deep sources:

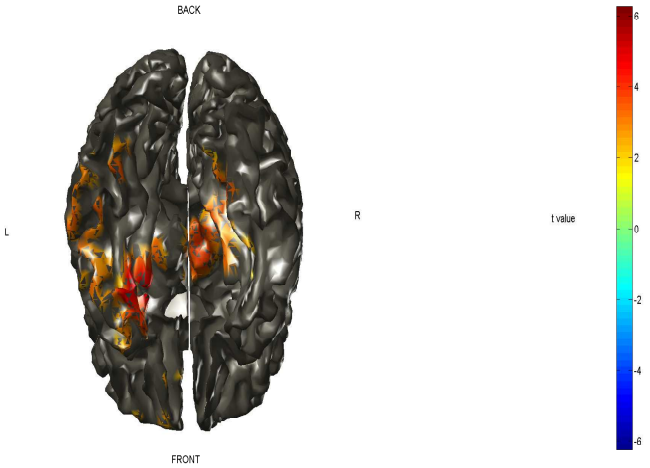

Figure 6.6: "Topographical" perspective of the source reconstruction.

Furthermore, the significant areas observed in this analysis confirm the physiological theories about the pathway of cardiac control signals: in fact, the cerebral peduncle and then the cerebellum are the exit areas of the vagus nerve. Furthermore, the cerebral peduncle is the link between the brainstem, through which the vagus nerve passes, and the thalamus, which, with the hypothalamus (which is included in the thalamus in the AAL), is a control area for the autonomic nervous system. Thalamus and hypothalamus are also part of the limbic system, which includes the hippocampus and the amygdala too.
The limbic system is a functional region of the brain that occupies parts of the cerebral cortex and basal ganglia of the cerebrum, the hypothalamus, the thalamus and the brain stem. It is the center of the brain that is responsible for our emotions, or feelings about ourselves and our place in the world.
The limbic system contains networks of nerve fibers that interconnect many nuclei with the various part of the brain. These fibers extend between the higher and lower brain centers. Their interconnections allow the system to receive and integrate information from a wide variety of stimuli, ranging from smells that reach our consciousness to visceral sensations of which we are not aware. They also allow a complex response, which can be initiated through the autonomic nervous system to cause what are termed psychosomatic disorders. These include tension, hypersecretion of acid in the stomach, headaches, and muscle spasms. The most severe form of response to an emotional state is cardiac arrest, which can be brought on by extreme fear or anxiety. On the more positive side, emotional responses may generate a feeling of warmth, security, and a sense of well-being. These responses are possible because of the connections between the limbic system and the higher center of thought within the cerebral cortex. By virtue of these connections we have the ability to be consciously aware of the emotional state of our lives [22].
Thus, this analysis is an example of how, using an internal targe stimulus, the autonomic data processing carried out by the brain can be actually evaluated and

analyzed. This new perspective on MEG (and EEG) data analysis could lead to uncover many hidden aspects on how our brain is able to handle such a high amount of information and to effectively control every body activity. The autonomic nervous system is definitely an amazing topic, whose better understanding might be a great source of inspiration in both information processing and automatic controls areas.
Nevertheless, a maybe deeper question arises naturally: since many autonomic functions, such as the heartbeat control, are actually carried out by the same brain area, i.e. the hypothalamus, that are cores of our self-awareness, where actually is the edge between autonomic and the somatic systems? Are the deepest functions of our organism really locked in an unreachable black-box or is there a way to consciously control them?
The answer to these questions is not trivial at all, but hopefully this work will be a hint for a research towards such direction.

References

[1] H-D. Park *et al.*, "Spontaneous fluctuations in neural responses to heartbeats predict visual detection", *Nature Neuroscience*, Apr. 2014, pp. 612-617.

[2] M. A. Gray *et al.*, "A cortical potential reflecting cardiac function", *PNAS*, Apr. 17, 2007, pp. 6818-6823.

[3] G. F. Wilson *et al.*, "Evoked Potential, Cardiac Blink and Respiration Measures of Pilot Workload in Air-to-Ground Missions", *Aviation, Space and Environmental Medicine*, Feb. 1994, pp. 100-105.

[4] A. Schulz *et al.*, "Cortisol rapidly affects amplitudes of heartbeat-evoked brain potentials - Implications for the contribution of stress to an altered perception of physical sensations?", *Psychoneuroendocrinology*, Jun. 2013, 38, pp. 2686-2693.

[5] S. Shao *et al.*, "Effect of pain perception on the heartbeat evoked potential", *Clinical Neurophysiology*, Mar. 2011, pp. 1838-1835.

[6] P. Montoya *et al.*, "Hearbeat evoked potentials (HEP): topography and influence of cardiac awareness and focus of attention", *Electroencephalography and clinical Neurophysiology*, 88 (1993), pp. 163-172.

[7] G. Dirlich *et al.*, "Topography and morphology of heart action-related EEG potentials", *Electroencephalography and clinical Neurophysiology*, 108 (1998), pp. 299-305.

[8] H. D. Critchley *et al.*, "Neural systems supporting interoceptive awareness", *Nature Neuroscience*, Feb. 2004, pp. 189-195.

[9] J. Terhaar *et al.*, "Heartbeat evoked potentials mirror altered body perception in depressed patients", *Clinical Neurophysiology*, 123 (2012), pp. 1950-1957.

[10] O. Pollatos *et al.*, "Accuracy of heartbeat perception is reflected in the amplitude of the heartbeat-evoked brain potential", *Psychophysiology*, 41 (2004), pp. 476-482.

[11] E. R. Kandel - J. H. Schwartz - T. M. Jessel, "Principles of Neural Science", *McGraw Hill*, 4th ed., 2000.

[12] R. Oostenveld *et al.*, "FieldTrip: open source software for advanced analysis of MEG, EEG, and invasive electrophysiological data, *Comput. Intell. Neurosci.*, 2011.

[13] J. Ashburner and K. J. Friston, "SPM", *Hum. Brain Mapp.*, 7 (1999), pp. 254–266.

[14] A. G. Ramakrishnan *et al.*, "Threshold - Independent QRS Detection Using the Dynamic Plosion Index", *IEEE Signal Processing Letters*, vol. 21, no. 5, May 2014, pp. 554-558.

[15] T. D. Wager *et al.*, "Increased sensitivity in neuroimaging analyses using robust regression", *NeuroImage*, 2005, 26, pp 99-113.

[16] E. Maris, R. Oostenveld, "Nonparametric statistical testing of EEG- and MEG-data", *Journal of Neuroscience Methods*, 164 (2007), pp. 177-190.

[17] R. C. Blair, W. Karnisky, "An alternative method for significance testing of waveform difference potentials", *Psychophysiology*, 30 (1993), pp. 518-524.

[18] C. R. Pernet *et al.*, "Cluster-based computational methods for mass univariate analyses of event-related brain/potentials field: A simulation study", *Journal of Neuroscience Methods*, (2014).

[19] G. Nolte, "The magnetic lead field theorem in the quasi-static approximation and its use for magnetoencephalography forward calculation in realistic volume conductors", *Phys Med Biol.*, 2003 Nov 21, 48 (22), pp. 3637-52 .

[20] B. D. Van Veen *et al*, "Localization of brain electrical activity via linearly constrained minimum variance spatial filtering", *IEEE Trans Biomed Eng*, Sep. 1997; 44 (9), pp. 867-80.

[21] N. Tzourio-Mazoyer et al., "Automated Anatomical Labeling of Activations in SPM Using a Macroscopic Anatomical Parcellation of the MNI MRI Single-Subject Brain", *NeuroImage*, 2002, 15, pp. 273-289.

[22] B. D. Wingerd, "The Human Body - concepts of anatomy & physiology", *Saunders College Publishing* , 1994.